MCB
Journals.ASM.org

A Protease-Independent Function for SPPL3 in NFAT Activation

Stefanie L. Makowski, Zhaoquan Wang, Joel L. Pomerantz

Department of Biological Chemistry, Institute for Cell Engineering, The Johns Hopkins University School of Medicine, Baltimore, Maryland, USA

The signal peptide peptidase (SPP)-related intramembrane aspartyl proteases are a homologous group of polytopic membrane proteins, some of which function in innate or adaptive immunity by cleaving proteins involved in antigen presentation or intracellular signaling. Signal peptide peptidase-like 3 (SPPL3) is a poorly characterized endoplasmic reticulum (ER)-localized member of this family, with no validated cellular substrates. We report here the isolation of SPPL3 in a screen for activators of NFAT, a transcription factor that controls lymphocyte development and function. We find that SPPL3 is required downstream of T cell receptor engagement for maximal Ca^{2+} influx and NFAT activation. Surprisingly, the proteolytic activity of SPPL3 is not required for its role in this pathway. SPPL3 enhances the signal-induced association of stromal interaction molecule 1 (STIM1) and Orai1 and is even required for the full activity of constitutively active STIM1 variants that bind Orai1 independently of ER Ca^{2+} release. SPPL3 associates with STIM1 through at least two independent domains, the transmembrane region and the CRAC activation domain (CAD), and can promote the association of the STIM1 CAD with Orai1. Our results assign a function in lymphocyte signaling to SPPL3 and highlight the emerging importance of nonproteolytic functions for members of the intramembrane aspartyl protease family.

The NFAT family of transcription factors regulates a variety of cellular functions by initiating new programs of gene expression in response to changes in intracellular Ca^{2+} levels. NFAT plays a critical role in the immune and nervous systems, in heart and bone development, and in other tissues (1, 2). In the adaptive immune system, NFAT regulates genes that control thymocyte development, T cell activation, T helper differentiation, and self-tolerance (3) and thus serves as a major determinant of how the immune system responds to pathogens and distinguishes between self and nonself.

T cell receptor (TCR) signaling activates NFAT activity through the Ca^{2+}-dependent phosphatase calcineurin, which dephosphorylates NFAT in the cytoplasm and allows NFAT to translocate to the nucleus to regulate target genes. TCR signaling elevates cytoplasmic Ca^{2+} concentrations by inducing store-operated Ca^{2+} entry (SOCE), a process in which inositol-1,4,5-triphosphate (IP_3)-mediated release of Ca^{2+} from the endoplasmic reticulum (ER) leads to the activation of Ca^{2+} channels in the plasma membrane, resulting in Ca^{2+} influx (4).

During SOCE, the drop in the ER Ca^{2+} concentration causes conformational changes in the EF hand and SAM domains of stromal interaction molecule 1 (STIM1), which reside in the ER lumen (5–9). These changes enhance STIM1 oligomerization and propagate across the transmembrane region into conformational changes that involve several cytoplasmic domains, resulting in the extension of coiled-coil domains, the exposure of the STIM1 Ca^{2+} release-activated Ca^{2+} (CRAC) activation domain (CAD; also called SOAR and Ccb9), which binds and activates Orai1, and the presentation of the STIM1 polybasic region, which interacts with negatively charged phospholipids in the plasma membrane (10–17). During this process, STIM1 oligomerizes further and translocates to ER–plasma membrane junctions called puncta (18, 19), where Orai1, the CRAC channel pore, accumulates (20–25). Although much is known about STIM1 and Orai1 function during SOCE (26, 27), the extent to which their induced interaction is modulated by auxiliary factors that influence the output of NFAT activity downstream of antigen receptor engagement remains unclear.

Signal peptide peptidase (SPP) and the SPP-like (SPPL) proteins belong to a group of intramembrane-cleaving aspartyl proteases whose biological functions are only beginning to emerge (28). The group, which includes SPP, SPPL2a, SPPL2b, SPPL2c, and SPPL3, is homologous to presenilins, which, as subunits of γ-secretase, have well-established roles in the processing of amyloid precursor protein, Notch, and other substrates (29). Several SPP/SPPL proteases have been linked to processes critical for innate or adaptive immunity. SPP generates peptides for presentation by HLA-E and major histocompatibility complex (MHC) class I and thus functions in both innate and adaptive immune surveillance by NK and T cells, respectively (30, 31). SPPL2a cleaves the N-terminal fragment (NTF) of the invariant chain (Ii; CD74) and is essential for the normal development of B cells and myeloid dendritic cells (32–34). SPPL2a has also been shown to cleave Fas ligand (FasL) to generate an intracellular domain (ICD) that negatively regulates B and T cell activation and proliferation downstream of antigen receptor triggering (35). Both SPPL2a and SPPL2b can cleave tumor necrosis factor alpha (TNF-α) to produce an ICD that elicits production of the proinflammatory cytokine interleukin 12 (IL-12) by bone marrow-derived dendritic

Received 5 September 2014 **Returned for modification** 28 October 2014
Accepted 31 October 2014

Accepted manuscript posted online 10 November 2014

Citation Makowski SL, Wang Z, Pomerantz JL. 2015. A protease-independent function for SPPL3 in NFAT activation. Mol Cell Biol 35:451–467. doi:10.1128/MCB.01124-14.

Address correspondence to Joel L. Pomerantz, joel.pomerantz@jhmi.edu.

Supplemental material for this article may be found at http://dx.doi.org/10.1128/MCB.01124-14.

doi:10.1128/MCB.01124-14

cells (36). Immunity-related functions of SPPL2c and SPPL3 are as yet unknown, and physiologically validated substrates for these proteins have not been identified.

To identify novel modulators of NFAT function, we adapted a transcriptional target-based expression cloning approach (37, 38) and isolated SPPL3 as an NFAT activator. We report here that SPPL3 modulates antigen receptor signaling to NFAT by promoting the optimal association of STIM1 and Orai1 during SOCE. Surprisingly, SPPL3 functions in this pathway in a protease-independent manner.

MATERIALS AND METHODS

Expression cloning screen. Pools of 100 cDNAs from a mouse thymus cDNA library (OriGene Technologies, Inc.) were screened as described previously (38), except that 20 ng of the $NFAT_4$-IFN-LUC construct was used as a reporter.

Expression constructs. Full-length SPPL3 cDNA in pCMV6-XL4 isolated from a mouse thymus cDNA library was cloned into pcDNA3 (Invitrogen) in frame with an N-terminal myc or FLAG tag. myc-SPPL3 was also cloned into pEBB. mCherry was cloned upstream of myc to create mCherry-myc-SPPL3 pcDNA3. Human SPP and SPPL2b cDNAs (OriGene) were cloned into pcDNA3 containing a C-terminal FLAG tag. For SPP, FLAG was encoded downstream of the KKXX ER retention motif. The SPPL3 D200A and D271A mutations were generated by PCR-based mutagenesis. Untagged full-length SPPL3 flanked by a 25-bp 5′ untranslated region (5′ UTR) and a 1,593-bp 3′ UTR was cloned into pEBB and was used for RNA interference (RNAi) rescue and 293T immunoprecipitation (IP) experiments. Rluc8 was cloned downstream of SPPL3 in pcDNA3, and 3 copies of the sequence LDASTFIRPALVTTS were inserted to extend the linker between SPPL3 and Rluc8.

Soluble mCherry was a gift from Mollie Meffert. Green fluorescent protein-tagged NFAT4 (GFP-NFAT4) (39) was a gift from Jun Liu. myc-PS1 pRK5 was a gift from Paul Worley. CRACM1.WT-myc-His and FLAG-CRACM1.E106Q pIRES2-EGFP (gifts from Monika Vig [20]) were subcloned into pcDNA3. Orai1-myc-Rluc8 was made by replacing the His tag in Orai1-myc-His with Rluc8. Wild-type (WT) myc-STIM1 pRK5 and myc-STIM1 D76A pRK5 (gifts from Paul Worley) (40) were subcloned into pcDNA3 such that the myc epitope was located downstream of the signal sequence cleavage site. PCR was used to generate the panel of myc-STIM deletion constructs diagramed in Fig. 8A and to introduce the 4EA (E-to-A mutations at residues 318, 319, 320, and 322 [15]), L251S, and L416S L423S (10) mutations into myc-STIM1 in pcDNA3. The STIM1 CAD (residues 342 to 448 [12]) was amplified by PCR and was cloned into pEBG downstream of glutathione *S*-transferase (GST). The linker between GST and CAD was extended by the insertion of five repeats of the sequence GGSGKD. Constitutively active phospholipase Cγ1 (PLCγ1 D1019L Y509A F510A) was a gift from Matilda Katan (41), and constitutively active calcineurin β2(1–401) was a gift from Jun Liu (42). CA-NFAT2 (plasmid 11102) (43), yellow fluorescent protein-tagged Orai1 (Orai1-YFP) (plasmid 19756), and STIM1-YFP (plasmid 19754) were obtained from Addgene. D1ER was a gift from Amy Palmer (GenBank accession no. AY796115 [44]).

Cell culture. HEK293T and human Jurkat T cells were grown as described previously (45). HeLa cells were cultured identically to HEK293T cells. Chicken DT40 B cells (from Tomohiro Kurosaki [46]) were grown in RPMI 1640 medium supplemented with 10% fetal bovine serum, 1% chicken serum, 100 U/ml each of penicillin and streptomycin, 2 mM glutamine, and 50 μM β-mercaptoethanol under humidified 5% CO_2 at 39.5°C.

HEK293T reporter assays. HEK293T reporter assays were performed as described previously (45, 47), except that 20 ng $NFAT_4$-IFN-LUC was used as the reporter. For FK506 treatment, the medium was replaced following transfection with a medium containing 10 nM FK506 (LC Laboratories). For Western blotting, corresponding Promega reporter lysis buffer lysates with equivalent β-galactosidase (β-gal) activities were incubated at 65°C for 15 min in the presence of SDS loading buffer and were separated by SDS-PAGE on 10% gels. Membranes were blotted with anti-myc (catalog no. sc-40; Santa Cruz) and anti-FLAG (M2; catalog no. IB13026; Eastman Kodak) antibodies using the Immun-Star WesternC ECL kit (Bio-Rad). The experiment for which results are shown in Fig. 1H was carried out as described above, except that HEK293T cells were transfected with 400 ng total DNA for reporter activity assessment. For Western blotting, HEK293T cells were plated at 5×10^5/well in 6-well plates and were transfected as described above. Cells were harvested as described previously (48), except that triplicate wells were pooled and resuspended in 350 μl modified buffer A, in which a protease inhibitor cocktail (catalog no. P8340; Sigma) was substituted for leupeptin, pepstatin A, and aprotinin. After the nuclear fraction was discarded, buffer D was added to the supernatant. Samples were incubated at 65°C for 15 min, loaded according to normalized β-gal activity, and separated by SDS-PAGE on a 10% gel.

Jurkat T cell reporter assays. Jurkat T cells were transfected as described previously (45), except that 1,500 ng $NFAT_4$-IFN-LUC was used as the reporter. For drug experiments, cells were treated with 10 nM FK506 24 h after transfection. Cells were stimulated with 1 μg/ml each of anti-CD3 (catalog no. 555329; BD Pharmingen) and anti-mouse IgG1 (catalog no. 553440; BD Pharmingen) 5 h prior to harvest. In some cases, anti-CD28 (catalog no. 555725; BD Pharmingen) was also used. Alternatively, cells were stimulated with 50 nM thapsigargin (catalog no. T9033; Sigma) plus 50 ng/ml phorbol myristate acetate (PMA) (catalog no. P1585; Sigma).

DT40 cell transfections. WT DT40 cells and IP_3 receptor (IP_3R) knockout (KO) cells were transfected using Nucleofector kit T (Lonza) and Nucleofector II (Amaxa) as described previously (49). A total of 23 μg DNA was used, including 10 μg $NFAT_4$-IFN-LUC, 5 μg CskA-lacZ, an expression vector for the indicated protein, and an empty parental vector to ensure equivalent total DNA. Lysates were assayed for luciferase and β-gal activities. For anti-IgM stimulation, cells were serum starved for 12 h prior to treatment with 3 μg/ml anti-IgM (catalog no. 8300-01; Southern Biotech) for 5 h.

Confocal microscopy. To assess NFAT nuclear translocation, HEK293T cells plated at 3.6×10^4/dish in 10-mm microwells of 35-mm glass-bottom petri dishes (catalog no. P35G-0-10-C; MatTek) were transfected 24 h later with 400 ng total DNA using TransIT-LT1 (Mirus Bio LLC). Cells were imaged 12 to 16 h later on an LSM 5 Pascal confocal microscope (Zeiss) at 37°C.

Anti-SPPL3 antibody design and production. GST-SPPL3 (amino acids 213 to 260) in pGEX-6P-1 (GE Healthcare) was transformed into Rosetta 2 or Rosetta 2(DE3) competent cells (Novagen) for isopropyl-β-D-thiogalactopyranoside (IPTG)-induced expression. The fusion protein was purified on glutathione-Sepharose 4 Fast Flow (GE Healthcare) by standard methods and was used by Covance Research Products, Inc., as described previously (50).

HEK293T immunoprecipitation. HEK293T cells were plated at 5×10^5/well in 6-well plates and were transfected 24 h later with 3 μg total DNA per well using *Trans*IT-LT1. The medium was changed 24 h later, and cells were harvested as described previously (50). For FLAG coimmunoprecipitation, samples were optionally precleared twice for 30 min each time. While 35 μl was saved as a whole extract, 350 μl were incubated with 0.8 to 1 μg of anti-FLAG antibody (catalog no. F7425; Sigma) for 2 to 3 h, followed by incubation with 7-μl bed volume of protein G-Sepharose 4 Fast Flow (GE Healthcare) for 1 to 2 h, all with rotation at 4°C. Beads were washed and were then eluted twice with 100 μg/ml FLAG peptide (catalog no. F3290; Sigma). Pooled eluates containing buffer D were incubated at 65° for 15 min and were analyzed by Western blotting with anti-myc, anti-FLAG, anti-SPPL3, or anti-GST (catalog no. G018; ABM) using the Pierce ECL substrate (Thermo Fisher). For GST pulldown, samples were precleared twice for 30 min each time with protein G-Sepharose. After incubation with glutathione-Sepharose 4 Fast Flow for 2.5 h, beads were washed and were resuspended in 30 μl 5× buffer D. Samples were incu-

bated at 65°C for 15 min and were analyzed by Western blotting with anti-FLAG and anti-GST (catalog no. sc-459; Santa Cruz) using a Pierce or Immun-Star WesternC ECL kit. For the experiments for which results are shown in Fig. 8D and E, the contents of 3 wells of a 6-well plate were pooled into one sample.

Calcium imaging by flow cytometry. HEK293T cells were plated at 5×10^5/well in 6-well plates and were transfected 24 h later with 2.5 μg total DNA per well using the *Trans*IT-LT1 reagent. Cells were analyzed 20 to 24 h after transfection. Pools of 3 wells were trypsinized and were washed with phosphate-buffered saline (PBS). After a 25-min incubation at room temperature with 7 μM Indo-1 AM (catalog no. I1226; Invitrogen) in cation-safe solution supplemented with 2 mM $CaCl_2$ and 0.1% bovine serum albumin (BSA) (51), cells were washed twice with Ca^{2+}-free buffer. Samples were stimulated with 1 μM thapsigargin (Sigma) and 2 mM $CaCl_2$.

Jurkat cells were also washed with PBS and were loaded with Indo-1 as indicated for HEK293T cells. Cells resuspended in Ca^{2+}-free buffer were treated either with 0.1 μg/ml anti-CD3 and anti-mouse IgG1, with 0.5 μg/ml anti-CD3, anti-CD28, and anti-mouse IgG1, or with 0.01 μM thapsigargin followed by 2 mM Ca^{2+} and 2 μM ionomycin (catalog no. I0634; Sigma). Data were collected on an LSR II flow cytometer (BD). Statistical calculations were carried out using data analyzed by FlowJo software (TreeStar). The Indo-1 ratio was manually calculated as a derived parameter, by dividing the Indo-1 Violet value by the Indo-1 Blue value. For HEK293T cell experiments, mean basal, peak, and plateau values were determined over a 2-s time slice gated on live, GFP-positive cells and were normalized to values for GFP-only cells. For Jurkat cell experiments, mean basal, peak, and plateau values were determined over a 2-s time slice gated on live cells, excluding cells with Indo-1 Blue values close to zero, and were normalized to values for control nontarget short hairpin RNA (shRNA)-expressing cells (shNT cells). The number of cells within the time slice ranged from ~150 to 650 for HEK293T cell experiments and from ~1,000 to 3,000 for Jurkat cell experiments. Means, standard deviations, and numbers of cells in the time slice were exported from FlowJo statistical analysis, and *P* values were calculated using means, standard errors of the means (SEM), and numbers of cells in the time slices in an unpaired, two-tailed *t* test calculator from GraphPad Prism. In the figures, error bars represent SEM and single asterisks represent a *P* value of <0.001. To determine the ER release rate following thapsigargin application or antibody stimulation, or the Ca^{2+} influx rate following the restoration of extracellular Ca^{2+}, slopes were calculated by dividing the change in the Indo-1 ratio by the time elapsed over an interval between two time points, A and B. The uncertainty in the slope was calculated as the difference between the maximum and minimum slopes (using mean Indo-1 ratio values ± SEM at A and B), divided by 2.

Lentivirus-mediated stable knockdown lines. Replication-incompetent lentiviral vector pLKO.1 expressing shRNA was packaged into HEK293T cells to infect HEK293T or Jurkat target cells, as described previously (50). HEK293T and Jurkat T cells were selected with 1 μg/ml and 0.5 μg/ml puromycin (Sigma), respectively. The Mission nontarget shRNA control vector (catalog no. SHC002; Sigma) (sense sequence, 5′-CAACAAGATGAAGAGCACCAA-3′; loop sequence, 5′-CTCGAG-3′) was used as a control. Hairpins targeting STIM1 and Orai1 were kindly provided by Rajini Rao (52). The SPPL3-specific shRNAs were shSPPL3-1 (sense sequence, 5′-GAACAAGATTTCCTTTGGT-3′; loop sequence, 5′-TTCAAGAGA-3′) and shSPPL3-2 (sense sequence, 5′-CCTGGTCTCCT ACTATGCTTT-3′; loop sequence, 5′-CTCGAG-3′.

To confirm protein knockdown, cells were lysed, and the protein concentration was determined as described previously (50). Samples containing SDS loading buffer were incubated at 65°C for 15 min and were resolved by Western blotting with anti-STIM1 (catalog no. 610954; BD Biosciences), anti-Orai1 (catalog no. AB9868; Millipore), anti-β-tubulin (catalog no. AA12.1; Developmental Studies Hybridoma Bank), anti-IκB kinase alpha (anti-IKKα) (catalog no. SC-7606; Santa Cruz), and anti-SPPL3. To determine RNA levels, RNA was isolated from SPPL3 knockdown Jurkat T cells using TRIzol reagent (Invitrogen) and was reverse transcribed using random hexamers (Qiagen), a deoxynucleoside triphosphate (dNTP) mixture (New England Biolabs [NEB]), RNase inhibitor (NEB), and Moloney murine leukemia virus (M-MLV) reverse transcriptase (Promega). Reverse transcription-quantitative PCR (RT-qPCR) was performed on a CFX Connect system (Bio-Rad) using Maxima Probe/ROX qPCR master mix (Fermentas) and TaqMan gene expression assay sets (Applied Biosystems) for human glyceraldehyde-3-phosphate dehydrogenase (GAPDH) (catalog no. 4352934), SPPL3 (catalog no. 00293370 and 01000610), IL-2 (catalog no. 00174114), TNF-α (catalog no. 01113624), gamma interferon (IFN-γ) (catalog no. 00989291), granulocyte-macrophage colony-stimulating factor (GM-CSF) (catalog no. 00929873), and FasL (catalog no. 00181225), and results were analyzed using the standard-curve method.

FRET. HEK293T cells plated at 2×10^5/dish in 35-mm glass-bottom petri dishes with 14-mm microwells (catalog no. P35G-0-14-C; MatTek) were TransIT-LT1 transfected 24 h later with 1 μg total DNA, including 500 ng D1ER and 200 ng mCherry-myc-SPPL3. Cells with similar mCherry intensities were used as a negative control. As described previously (53, 54), 40 to 48 h after transfection, cells were washed twice in Ca^{2+}-free Hanks balanced salt solution (HBSS) (1× HBSS, 2 g/liter D-glucose, 20 mM HEPES, 1 g/liter $MgCl_2 \cdot 6H_2O$, 1 g/liter $MgSO_4 \cdot 7H_2O$ [pH 7.4]) and were stimulated with 4 μM thapsigargin followed by 5 μM ionomycin plus 5 mM EGTA. Imaging was performed on an Axiovert 200M microscope (Zeiss) using a 40× oil immersion objective lens (numerical aperture [NA], 1.3) and MetaFluor software. The filter sets used have been described previously (55). The fluorescence resonance energy transfer (FRET) ratio (*R*) was calculated as (FRET channel emission intensity − FRET channel emission intensity of background)/(cyan fluorescent protein [CFP] channel emission intensity − CFP channel emission intensity of background).

BRET assays. HEK293T cells were plated at 9×10^4/well in 24-well plates and were transfected 24 h later with 500 ng total DNA per well using *Trans*IT-LT1 or 350 ng total DNA per well using $CaPO_4$. The medium was changed 20 to 24 h later, and cells were harvested 40 to 44 h after transfection. In a procedure modified from that of Hamdan et al. (56), after trypsinization, HEK293T cells were resuspended in 250 μl Dulbecco's PBS, 1× (DPBS; Gibco). Measurements were collected using the TriStar LB 941 multimode microplate reader (Berthold Technologies). Fluorescence was measured in black 96-well plates by exciting cells at 485 nm and recording emission at 535 nm, while bioluminescence resonance energy transfer (BRET) was measured in white 96-well plates 10 to 40 min after the addition of coelenterazine-h to a final concentration of 5 μM (catalog no. S2011; Promega). Rluc8 emission was detected over 1 s at 480 nm, and YFP emission was detected over 1 s at 540 nm. To calculate milli-BRET (mBRET) values, background-corrected YFP/Rluc8 ratios of Rluc8-only samples were subtracted from corresponding ratios of Rluc8-plus-YFP samples, and the difference was multiplied by 1,000. Acceptor/donor ratios were calculated by dividing corrected YFP fluorescence by Rluc8 activity. Jurkat cells transfected with 3 μg total DNA using *Trans*IT-LT1 as described above were resuspended in 200 μl DPBS and were treated with 1 μg/ml IgG or anti-CD3 plus IgG. Following the addition of 5 μM coelenterazine-h, BRET was measured as described above.

Subcellular fractionation. For each time point, 1.2×10^7 control or SPPL3-knockdown Jurkat cells were either left unstimulated or treated with 1 μg/ml anti-CD3 and anti-mouse IgG1 at a density of 1.2×10^6/ml. Samples were plunged into an ice water bath, centrifuged at 423 × *g* for 5 min, and washed with cold PBS. Cell pellets were resuspended in 500 μl hypotonic lysis buffer (10 mM HEPES [pH 7.9], 1.5 mM $MgCl_2$, 10 mM KCl, 0.5 mM dithiothreitol [DTT]) supplemented with protease inhibitor cocktail and were incubated for at least 30 min. After 15 strokes with a prechilled Dounce homogenizer (loose pestle A), cells were spun at 228 × *g* for 5 min. The supernatant was saved as the cytoplasmic fraction. Nuclear pellets were resuspended in 50 μl buffer C as described previously (38). Equal protein samples containing SDS loading buffer were incu-

bated at 65° for 15 min and were resolved by Western blotting with anti-NFAT1 (catalog no. ab2722; Abcam), anti-caspase-3 (catalog no. 9662; Cell Signaling Technology), and anti-Oct-1 (catalog no. MAB5434; Millipore).

RESULTS

SPPL3 is a specific NFAT activator. To identify unrecognized modulators of the signaling pathway to NFAT, we used a transcriptional target-based expression cloning approach (37, 38). Pools of clones from a mouse thymus cDNA expression library were cotransfected at a complexity of 100 cDNAs per pool with an NFAT-responsive luciferase reporter, $NFAT_4$-IFN-LUC, into HEK293T cells and were assayed for the ability to activate the reporter 3-fold or more relative to the empty expression vector. From one positive pool, sib selection to identify the individual clone responsible for the pool's activity led to the purification of a cDNA encoding SPPL3. Transient expression of SPPL3 in HEK293T cells activated the NFAT reporter in a dose-dependent manner (Fig. 1A). Treatment with FK506, an inhibitor of calcineurin, completely abrogated SPPL3 activity (Fig. 1A), suggesting the dependence of SPPL3 activity on endogenous NFAT signaling pathway components. SPPL3 failed to activate a mutated reporter with disrupted NFAT-binding sites and an NF-κB-responsive reporter and only minimally activated an AP-1 reporter (Fig. 1B). Similar results were observed in Jurkat T cells (Fig. 1C and D).

To independently assay NFAT activation, we assessed the effect of SPPL3 expression on the nuclear translocation of GFP-NFAT in HEK293T cells. GFP-NFAT localized to the cytoplasm in control cells expressing mCherry alone, but coexpression with mCherry-myc-SPPL3 induced nuclear translocation (Fig. 1E). The localization pattern of mCherry-myc-SPPL3 was consistent with previous work showing that overexpressed SPPL3 localizes to the ER or the Golgi apparatus (36, 57).

We compared the activity of SPPL3 to those of several related members of the intramembrane aspartyl protease family (30, 58, 59). SPPL3 displayed much higher activity in the NFAT luciferase reporter assay than SPP, SPPL2b, or PS1 (Fig. 1F and G), suggesting a unique capability for this family member. To test whether the putative proteolytic activity of SPPL3 was required for NFAT activation, we mutated SPPL3 residues D200 and D271, which occupy the YD and GXGD active-site motifs shared by intramembrane aspartyl proteases (60). The mutation of D271 has been shown previously to abolish SPPL3 proteolytic activity (61). Changing D200 and D271 to alanine in SPPL3 had no effect on NFAT stimulation (Fig. 1H), suggesting that SPPL3 signaling to NFAT is independent of protease activity.

SPPL3 is required for NFAT activation by TCR signaling. To test whether SPPL3 is required at endogenous levels for receptor-induced signaling to NFAT, we stably knocked down SPPL3 expression in Jurkat T cells by lentivirus-mediated RNAi and assayed the effect on TCR-stimulated NFAT reporter activation. Two different shRNAs targeting SPPL3 decreased anti-CD3-induced NFAT reporter activation at least 4-fold from that observed with the control nontarget shRNA (Fig. 2A). These hairpins, shSPPL3-1 and shSPPL3-2, stably knocked down SPPL3 by 54% and 59% at the RNA level and by 59% and 77% at the protein level, respectively (Fig. 2B and C) without any effect on pathway components STIM1 and Orai1. Analysis of nuclear and cytoplasmic fractions revealed reduced anti-CD3-induced nuclear translocation and dephosphorylation of endogenous NFAT1 in SPPL3 knockdown cells relative to control cells (Fig. 2D). The TCR-mediated upregulation of several NFAT-dependent target genes (62), including TNF-α, GM-CSF, IFN-γ, and FasL, was also reduced in SPPL3 knockdown cells as measured by RT-qPCR (see Fig. S1 in the supplemental material). SPPL3 knockdown also reduced NFAT activation by anti-CD3 plus anti-CD28 cross-linking by 3.3-fold (Fig. 2E) and reduced NF-κB activation by the same stimulus by 1.7-fold (Fig. 2F). To validate RNAi specificity, we expressed hairpin-resistant murine SPPL3 in human Jurkat SPPL3 knockdown lines. At levels that did not activate NFAT in the absence of stimulation, SPPL3 rescued anti-CD3-mediated NFAT activation in SPPL3 knockdown cells to the level seen in control cells (Fig. 2G). Moreover, SPPL3 D200A D271A also rescued NFAT activation in SPPL3 knockdown cells (Fig. 2G). These experiments indicate that endogenous SPPL3 is required for optimal TCR signaling to NFAT and suggest that the putative aspartyl protease activity of SPPL3 is not required for its role in this pathway.

To further explore the dependence of TCR signaling to NFAT on SPPL3 expression levels, we titrated SPPL3 in wild-type Jurkat T cells. As shown in Fig. 2H, increasing SPPL3 levels potently enhanced the magnitude of NFAT activation following anti-CD3 treatment. These results confirm that the extent of TCR signaling to NFAT is highly dependent on the levels of SPPL3 expression.

SPPL3 is required for optimal TCR-induced Ca^{2+} influx. To resolve where SPPL3 functions in the TCR pathway, we took advantage of several gain-of-function mutants. During TCR signaling, PLCγ converts phosphatidylinositol-4,5-bisphosphate into diacylglycerol and IP_3; the latter acts on IP_3 receptors to induce Ca^{2+} release from the ER during SOCE. Transient expression of constitutively active PLCγ1 (41) in control cells robustly activated the NFAT reporter but elicited reduced NFAT activation in SPPL3 knockdown Jurkat T cells (Fig. 3A), indicating a requirement for SPPL3 downstream of PLCγ. This effect could be rescued by restoration of SPPL3 expression (Fig. 3A). Since SPPL3 knockdown cells displayed reduced dephosphorylation and nuclear translocation of endogenous NFAT1 (Fig. 2D), we suspected that SPPL3 would act upstream of calcineurin. Consistent with this, both constitutively active calcineurin (42) and NFAT2 (43) stimulated reporter activity equally well in control and SPPL3 knockdown cells (Fig. 3B and C), suggesting that SPPL3 acts upstream of calcineurin during signaling.

In the TCR pathway, calcineurin activity depends on the SOCE-mediated increase in cytoplasmic Ca^{2+} levels. To test whether SPPL3 acts upstream or downstream of receptor-induced Ca^{2+} influx, we assessed anti-CD3-mediated changes in cytoplasmic Ca^{2+} levels in SPPL3 knockdown and control Jurkat T cells using the ratiometric Ca^{2+} indicator Indo-1 in a flow cytometry assay. SPPL3 knockdown by both hairpins shSPPL3-1 and shSPPL3-2 resulted in statistically significant reductions in the anti-CD3-induced Ca^{2+} influx peak (13% and 14%, respectively) and Ca^{2+} influx plateau (16% and 17%) compared to those for the control shNT line (Fig. 3D; see also Fig. S2A in the supplemental material). The rate of Ca^{2+} influx was lower in SPPL3 knockdown cells by 44% (shSPPL3-1) and 40% (shSPPL3-2) (Fig. 3D; see also Fig. S2C). While the shSPPL3-1 cell line displayed a 14% reduction in the anti-CD3-induced ER Ca^{2+} release peak, the shSPPL3-2 cell line displayed only a 3% reduction in this parameter (Fig. 3D; see also Fig. S2A). The effects of SPPL3 knockdown

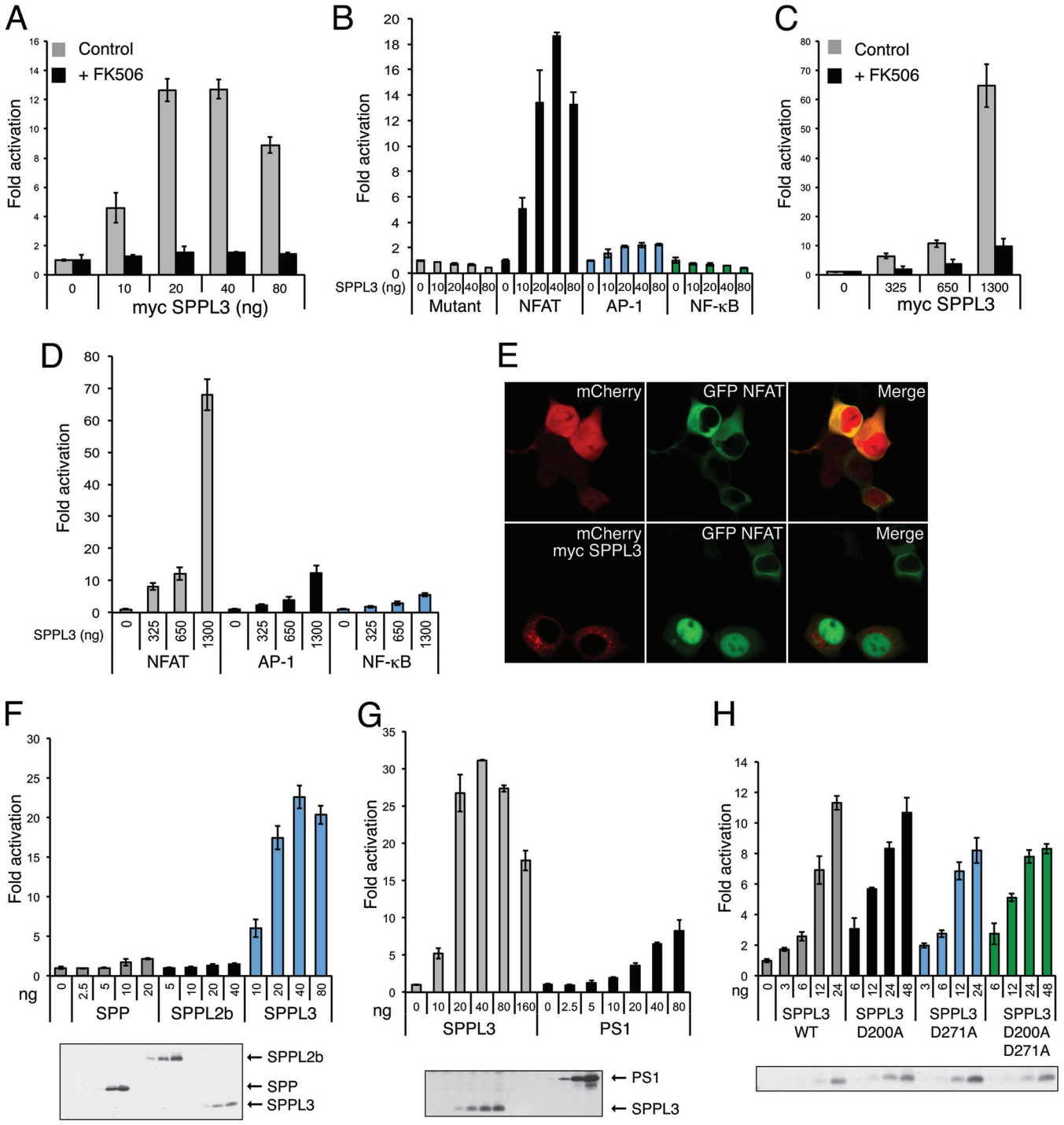

FIG 1 SPPL3 activates NFAT. (A) $NFAT_4$-IFN-LUC reporter activity in HEK293T cells transfected with myc-SPPL3 and either left untreated or treated with 10 nM FK506 for 24 h. (B) Luciferase activities of MUT-IFN-LUC (mutant), $NFAT_4$-IFN-LUC (NFAT), $AP\text{-}1_4$-IFN-LUC (AP-1), and $Ig\kappa_2$-IFN-LUC (NF-κB) reporters in HEK293T cells transfected with myc-SPPL3. (C) $NFAT_4$-IFN-LUC reporter activity in Jurkat T cells transfected with myc-SPPL3 and either left untreated or treated with 10 nM FK506 for 24 h. *x* axis units are nanograms. (D) Luciferase activities of $NFAT_4$-IFN-LUC (NFAT), $AP\text{-}1_4$-IFN-LUC (AP-1), and $Ig\kappa_2$-IFN-LUC (NF-κB) reporters in Jurkat T cells transfected with myc-SPPL3. (E) Confocal microscopy of GFP-NFAT4 nuclear localization in HEK293T cells cotransfected with mCherry or mCherry-myc-SPPL3. (F to H) $NFAT_4$-IFN-LUC reporter activity in HEK293T cells transfected with SPP-FLAG, SPPL2b-FLAG, and FLAG-SPPL3 (F), myc-SPPL3 and myc-PS1 (G), or WT myc-SPPL3 and catalytically inactive mutants (H). Western blots with an anti-FLAG (F) or anti-myc (G and H) antibody indicate similar expression levels.

were smaller than those achieved by knockdown of STIM1 and Orai1, two well-established mediators of SOCE, which reduced the ER Ca^{2+} release peak by 21% and 42%, respectively, the Ca^{2+} influx peak by 43% and 47%, the Ca^{2+} influx plateau by 36% and 36%, and the Ca^{2+} influx rate by 85% and 91%, respectively (Fig. 3D; see also Fig. S2A). Control and SPPL3 knockdown Jurkat T cells were also treated with anti-CD3 in the presence of anti-CD28 costimulation, which potentiates signaling from the TCR to

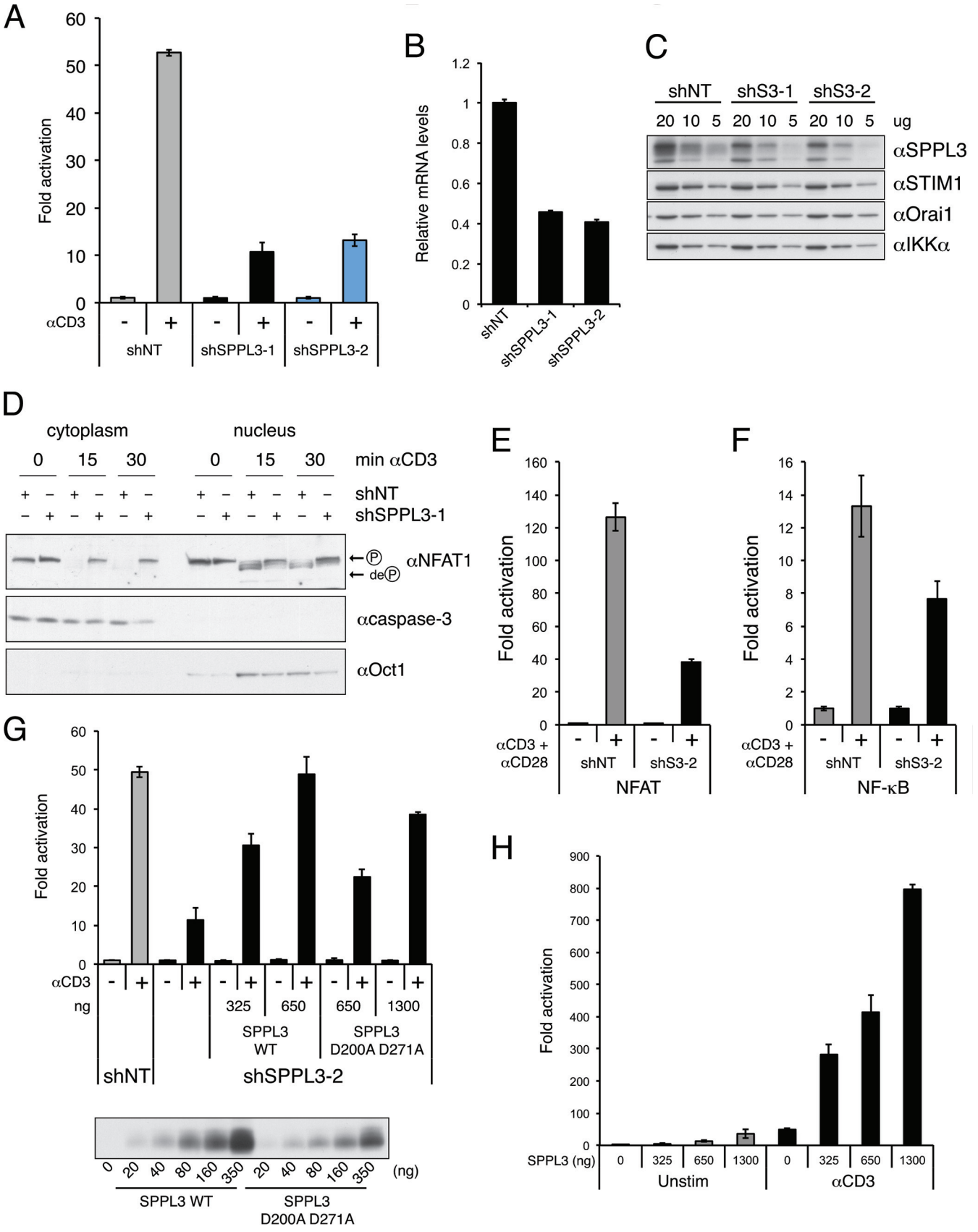
A
Fold activation
αCD3
shNT
shSPPL3-1
shSPPL3-2
B
Relative mRNA levels
shNT
shSPPL3-1
shSPPL3-2
C
shNT
shS3-1
shS3-2
ug
αSPPL3
αSTIM1
αOrai1
αIKKα
D
cytoplasm
nucleus
min αCD3
shNT
shSPPL3-1
αNFAT1
αcaspase-3
αOct1
E
Fold activation
αCD3 + αCD28
shNT
shS3-2
NFAT
F
Fold activation
αCD3 + αCD28
shNT
shS3-2
NF-κB
G
Fold activation
αCD3
ng
SPPL3 WT
SPPL3 D200A D271A
shNT
shSPPL3-2
(ng)
SPPL3 WT
SPPL3 D200A D271A
H
Fold activation
SPPL3 (ng)
Unstim
αCD3

NFAT. As shown in Fig. 3E, shSPPL3-1 knockdown cells displayed statistically significant reductions in the anti-CD3- and anti-CD28-induced Ca^{2+} influx peak and plateau (reductions of 16% and 11%, respectively) (Fig. 3E; see also Fig. S2D in the supplemental material). The rate of Ca^{2+} influx was 26% lower in shSPPL3-1 cells than in shNT cells (Fig. 3E; see also Fig. S2F). Similar reductions in these parameters were observed with the shSPPL3-2 cell line (data not shown). While the shSPPL3-1 cell line showed a 15% reduced ER Ca^{2+} release peak, no significant reduction in this parameter was observed with the shSPPL3-2 cell line following treatment with both anti-CD3 and anti-CD28 (Fig. 3E; see also Fig. S2D) (data not shown). Together, these results suggest that SPPL3 functions to enhance Ca^{2+} influx and sustain elevated cytoplasmic Ca^{2+} levels following TCR engagement.

We also treated control and SPPL3 knockdown T cells with thapsigargin, which promotes ER Ca^{2+} release by inhibiting the sarcoplasmic/ER Ca^{2+} ATPase (SERCA) pump, which is responsible for ER Ca^{2+} loading. SPPL3 knockdown cells displayed 51% (shSPPL3-1) and 48% (shSPPL3-2) reductions in the passive ER release rate and an ER release peak that was reduced by 20% in the shSPPL3-1 line and 10% in the shSPPL3-2 line (Fig. 3F; see also Fig. S2G and H in the supplemental material). The resulting Ca^{2+} influx peak was reduced by 9% (shSPPL3-1) and 21% (shSPPL3-2), while the influx plateau was reduced by 13% (shSPPL3-1) and 28% (shSPPL3-2) (Fig. 3F; see also Fig. S2G). The data suggest that in the absence of TCR engagement, SPPL3 contributes to the passive release of Ca^{2+} from the ER, which is normally opposed by SERCA pump activity.

We next assessed the effect of SPPL3 overexpression on ER Ca^{2+} release and the resultant Ca^{2+} influx by using HEK293T cells, which have high transfection efficiency. We found that SPPL3 overexpression elevated basal cytoplasmic Ca^{2+} levels and enhanced Ca^{2+} influx in a dose-dependent manner (Fig. 4A; see also Fig. S3A in the supplemental material). Furthermore, SPPL3 overexpression dampened the release of ER Ca^{2+} stores after thapsigargin treatment in the absence of extracellular Ca^{2+} (Fig. 4B; see also Fig. S3C to E), suggesting that overexpressed SPPL3 was sufficient to induce Ca^{2+} release from the ER prior to thapsigargin application. To assess the effect of SPPL3 on ER Ca^{2+} levels directly, we used the ER-targeted Ca^{2+} sensor D1ER (44), which exhibits FRET at the high basal ER Ca^{2+} concentration but whose FRET ratio diminishes as the ER Ca^{2+} concentration drops during ER Ca^{2+} release. High mCherry-myc-SPPL3 overexpression was sufficient to lower the D1ER FRET, compared to that observed for control cells expressing mCherry, and occluded the response in the FRET assay to thapsigargin treatment (Fig. 4C and D), consistent with the conclusion that SPPL3 overexpression can induce ER Ca^{2+} release.

SPPL3 activity does not require IP_3 receptors but does require STIM1. We hypothesized that when overexpressed, SPPL3 might promote ER Ca^{2+} release through an interaction with IP_3 receptors (IP_3Rs), since presenilin mutations found in familial Alzheimer's disease (AD) can enhance IP_3R gating (63). To test this possibility, we overexpressed SPPL3 in DT40 cells deficient in all three IP_3R isoforms (46), which fail to activate NFAT following anti-IgM antigen receptor cross-linking (Fig. 5A). SPPL3 stimulated NFAT activity in the absence of IP_3R, arguing against the modulation of IP_3R activity as a possible mechanism for SPPL3 activation of NFAT (Fig. 5B).

In the ER, STIM1 senses decreases in ER Ca^{2+} levels and undergoes conformational changes that allow it to bind to and activate the Orai1 CRAC channel at the plasma membrane. To test whether STIM1 was required for the activity of overexpressed SPPL3, we knocked down STIM1 in HEK293T cells by lentivirus-mediated RNAi. STIM1-deficient cells were defective in SPPL3-mediated NFAT activation (Fig. 5C; see also Fig. S5 in the supplemental material), consistent with the possibility that SPPL3 overexpression activates NFAT by promoting ER Ca^{2+} release upstream of STIM1 activation.

SPPL3 is required for the optimal inducible association of STIM1 and Orai1 following TCR engagement. The reduced Ca^{2+} influx observed in SPPL3 knockdown cells following TCR cross-linking (Fig. 3D and E) suggested that the TCR-induced association of STIM1 and Orai1 might be suboptimal in these cells. To test this possibility, we developed a bioluminescence resonance energy transfer (BRET) assay for STIM1 and Orai1 binding using STIM1-YFP and Orai1-myc-Rluc8 fusions, since the inducible association of endogenous STIM1 and Orai1 was not detectable in immunoprecipitation studies using available antibodies. In this assay, live cells are incubated with coelenterazine-h, a substrate of the *Renilla* luciferase derivative Rluc8. Energy generated by the reaction of Rluc8 with its substrate can be transferred to a YFP acceptor, provided the distance between the donor and acceptor is 100 Å or less (56). The resultant YFP fluorescence can be quantitated in a luminometer with appropriate emission filters. We monitored the anti-CD3-induced BRET between STIM1-YFP and Orai1-myc-Rluc8 in control and SPPL3 knockdown Jurkat T cells. Treatment of control T cells with anti-CD3 induced BRET between STIM1-YFP and Orai1-myc-Rluc8, which was sustained for the 35-min duration of the assay, while the control anti-IgG treatment did not induce BRET (Fig. 6A). In SPPL3 knockdown cells, anti-CD3 treatment induced BRET between STIM1-YFP and

FIG 2 SPPL3 is required for TCR-induced NFAT activation. (A) $NFAT_4$-IFN-LUC reporter activity in stable SPPL3 knockdown (shSPPL3-1 or shSPPL3-2) or control (shNT) Jurkat T cells stimulated with 1 μg/ml anti-CD3 for 5 h. (B) RT-qPCR demonstrates 54% and 59% knockdown of SPPL3 mRNA in the shSPPL3-1 and shSPPL3-2 lines, respectively, compared to the level in the control shNT line. (C) Western blot analysis with anti-SPPL3 illustrates 59% and 77% knockdown of SPPL3 protein in the shSPPL3-1 and shSPPL3-2 lines, respectively, compared to the level in the control shNT line. (D) Analysis of cytoplasmic and nuclear fractions from shNT and shSPPL3-1 lines demonstrates reduced dephosphorylation and nuclear translocation of endogenous NFAT1 following anti-CD3 treatment in the shSPPL3-1 line. To equalize protein loading in all lanes, each nuclear extract sample contains ~6-fold more cell equivalents than its corresponding cytoplasmic extract. In unstimulated cells, therefore, ~86% of the total phosphorylated NFAT1 species fractionates into the cytoplasmic extract, while ~14% fractionates into the nuclear extract. (E) $NFAT_4$-IFN-LUC (NFAT) reporter activities in stable SPPL3 knockdown Jurkat T cells stimulated with 1 μg/ml anti-CD3 plus anti-CD28 for 5 h. (F) $Ig\kappa_2$-IFN-LUC (NF-κB) reporter activities in stable SPPL3 knockdown Jurkat T cells stimulated with 1 μg/ml anti-CD3 plus anti-CD28 for 5 h. (G) (Top) $NFAT_4$-IFN-LUC reporter activity in control (shNT) or stable SPPL3 knockdown (shSPPL3-2) Jurkat T cells stimulated with 1 μg/ml anti-CD3 for 5 h. shSPPL3-2 Jurkat T cells were transfected with WT or mutant hairpin-resistant murine SPPL3 to test for rescue of the RNAi effect. (Bottom) Western blot of lysates from HEK293T cells transfected with WT SPPL3 or SPPL3 D200A D271A and probed with anti-SPPL3. Expression of the double mutant is ~50 to 60% lower than that of the WT protein at the identical ng level of transfected expression vector. (H) $NFAT_4$-IFN-LUC reporter activity in Jurkat T cells transfected with myc-SPPL3 and either left untreated (Unstim) or stimulated with 1 μg/ml anti-CD3 for 5 h.

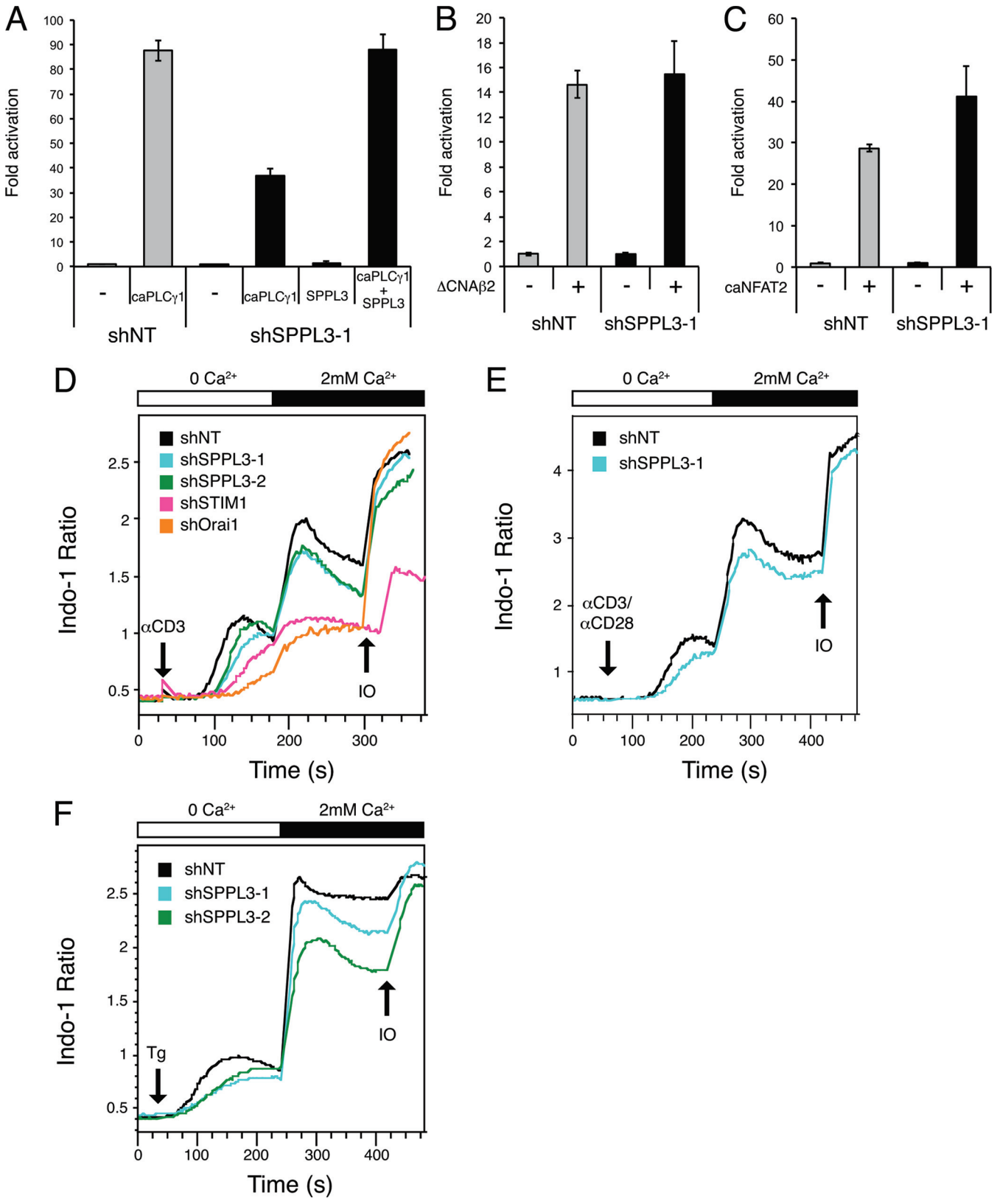

FIG 3 SPPL3 functions downstream of PLCγ and upstream of Ca^{2+} influx. (A to C) Control (shNT) and SPPL3 knockdown (shSPPL3-1) Jurkat T cell lines were transfected with constitutively active (ca) mutants of PLCγ1 (A), calcineurin (B), or NFAT2 (C) and were assayed for $NFAT_4$-IFN-LUC reporter activity. In panel A, SPPL3 knockdown cells were also cotransfected with hairpin-resistant murine SPPL3 to test for rescue of the RNAi effect. (D) Indo-1 Ca^{2+} measurements in control (shNT), SPPL3 knockdown (shSPPL3-1 or shSPPL3-2), STIM1 knockdown (shSTIM1), or Orai1 knockdown (shOrai1) Jurkat T cell lines washed in Ca^{2+}-free buffer and treated with 0.1 μg/ml anti-CD3 followed by 2 mM Ca^{2+} and 2 μM ionomycin. (E) The same experiment as for panel D except that cells were stimulated with 0.5 μg/ml anti-CD3 and anti-CD28 followed by 2 mM Ca^{2+} and 2 μM ionomycin. (F) The same experiment as for panel D except that cells were treated with 0.01 μM thapsigargin followed by 2 mM Ca^{2+} and 2 μM ionomycin. Data in panels D through F represent the results of experiments performed at least twice.

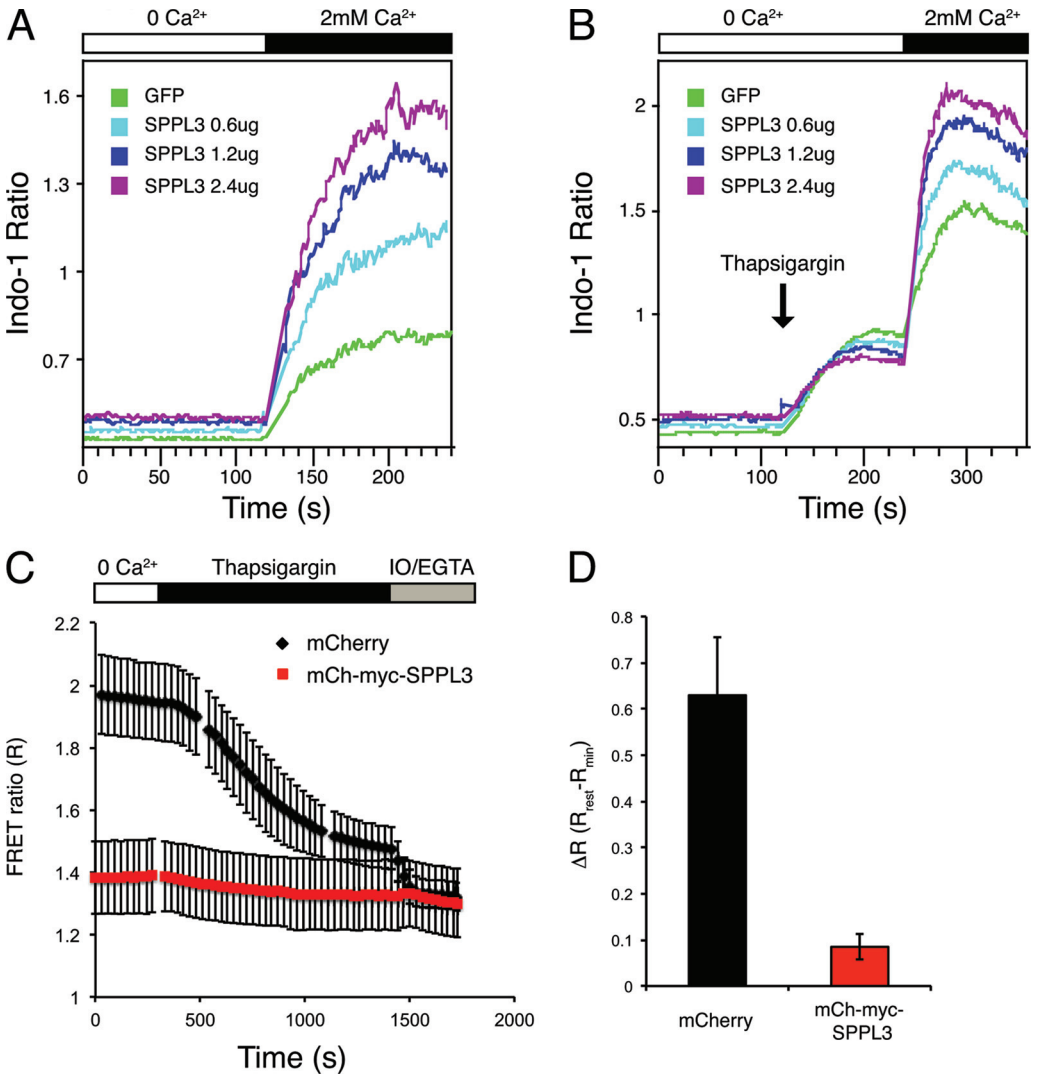

FIG 4 Overexpression of SPPL3 induces ER Ca^{2+} release and Ca^{2+} influx. (A and B) Indo-1 Ca^{2+} measurements in HEK293T cells transfected with GFP alone or with GFP plus myc-SPPL3. Cells washed in Ca^{2+}-free buffer were treated with 2 mM Ca^{2+} (A) or 1 μM thapsigargin followed by 2 mM Ca^{2+} (B). Samples were gated on GFP for kinetic analysis. Data represent the results of experiments performed at least twice. (C) D1ER Ca^{2+} measurements in HEK293T cells transfected with mCherry or mCherry-myc-SPPL3. Cells washed in Ca^{2+}-free buffer were treated with 4 μM thapsigargin followed by 5 μM ionomycin and 5 mM EGTA. (D) Quantification of the data shown in panel C by calculating the difference between resting and minimum FRET ratios.

Orai1-myc-Rluc8; however, the level of induction was significantly lower than that for control cells (Fig. 6A) for the duration of the assay. The results indicate that SPPL3 is required for optimal interaction between STIM1 and Orai1 following TCR triggering.

SPPL3 is required for maximal activity of activated STIM1 variants. During SOCE, the drop in ER Ca^{2+} levels leads to conformational changes in STIM1 that activate the protein for Orai1 binding. This process is driven by the dissociation of Ca^{2+} from the cEF hand in the ER lumen, leading to STIM1 oligomerization, and subsequent conformational changes in cytosolic STIM1 domains that enable STIM1 to move stably to puncta and interact with and activate Orai1 (26, 64, 65). Several constitutively active variants of STIM1 that harbor mutations that convert STIM1 into an active conformation independently of ER Ca^{2+} release have been reported. To probe whether SPPL3 functions after the conversion of STIM1 to an active conformation, at a step subsequent to ER Ca^{2+} release, we tested whether several constitutively active STIM1 variants depend on SPPL3 for their ability to activate NFAT.

We first tested whether the D76A mutant of STIM1 could bypass a requirement for SPPL3. This mutation in the cEF hand of STIM1 decreases its affinity for Ca^{2+} and mimics the conversion to an active STIM1 conformation normally induced by reduced ER Ca^{2+} levels. Transient expression of STIM1 D76A potently activated the NFAT reporter in control Jurkat T cells but, surprisingly, elicited reduced NFAT activation in SPPL3 knockdown T cells (Fig. 6B), indicating that the D76A variant depends on SPPL3 for optimal activity. The defective STIM1 D76A activity observed in SPPL3 knockdown cells could be rescued by restoration of SPPL3 expression, verifying that the knockdown phenotype was due to SPPL3 deficiency (Fig. 6B). Next, we tested the activities of three hyperactive STIM1 variants with mutations in inhibitory cytosolic domains that normally keep STIM1 inactive in the basal state: the 4EA (15), L251S (10), and L416S L423S (10) mutations.

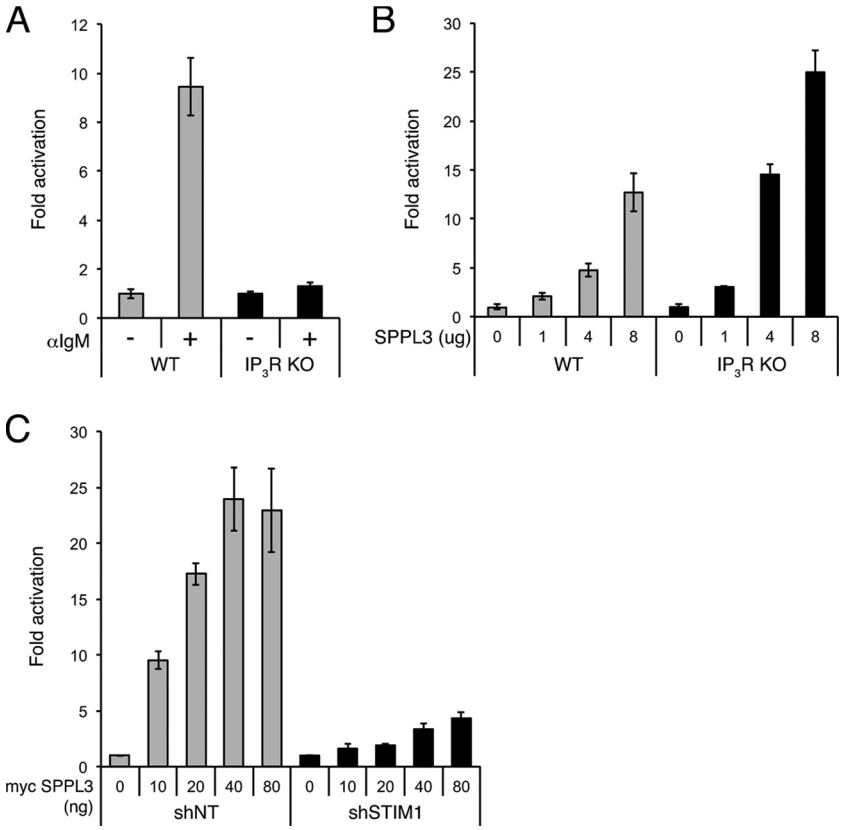

FIG 5 SPPL3 requires STIM1 but not IP_3R for activity. (A and B) NFAT luciferase activity of WT or IP_3R KO DT40 cells stimulated with 3 μg/ml anti-IgM for 5 h (A) or transfected with myc-SPPL3 (B). (C) HEK293T cells in which STIM1 was stably knocked down were transfected with myc-SPPL3 and were assayed for NFAT luciferase activity.

Interestingly, each of these constitutively active STIM1 variants was more active in control Jurkat T cells than in SPPL3 knockdown T cells (Fig. 6C to E), and their phenotype in SPPL3 knockdown cells could be rescued by SPPL3 expression, further supporting the notion that SPPL3 is required for optimal STIM1 activity even after the conversion of STIM1 to an active conformation. The hyperactivity of these STIM1 mutants results from the constitutive exposure of the STIM1 CAD, which binds to and activates Orai1. Therefore, we tested whether NFAT activation by a cytoplasmically expressed CAD was affected by SPPL3 deficiency. Indeed, expression of a GST-CAD fusion protein induced less NFAT activity in SPPL3 knockdown Jurkat T cells than in control cells, and this effect could be rescued by restoration of SPPL3 expression (Fig. 6F). These results suggest that SPPL3 functions in the TCR pathway at a step subsequent to ER Ca^{2+} release following the conversion of STIM1 to an active conformation.

SPPL3 associates with STIM1 and can promote the binding of the CAD to Orai1. To investigate how SPPL3 influences STIM1 action on Orai1, we first tested whether SPPL3 can associate with STIM1. When coexpressed in HEK293T cells, SPPL3 associated robustly with STIM1, as assayed by coimmunoprecipitation (Fig. 7A). To probe binding between SPPL3 and STIM1 in live cells, we assayed BRET between SPPL3-Rluc8 and STIM1-YFP in HEK293T cells. We used the Ypet variant of YFP at comparable levels of expression to gauge nonspecific BRET with SPPL3-Rluc8. STIM1-YFP displayed specific BRET with SPPL3-Rluc8 in a dose-dependent manner (Fig. 7B), supporting the conclusion that SPPL3 and STIM1 can associate in live cells.

To assess whether SPPL3 could influence STIM1 binding to Orai1, we performed a coimmunoprecipitation assay in which myc-STIM1 is coexpressed in HEK293T cells with the dominant negative mutant FLAG-Orai1 E106Q, which binds more robustly and is less toxic than WT Orai1 in this assay. Indeed, coexpression of SPPL3 did augment the interaction between STIM1 and Orai1 (Fig. 7C). Interestingly, SPPL3 coexpression also improved the association of STIM1 D76A with Orai1 (Fig. 7C), a finding consistent with a potential role for SPPL3 downstream of ER Ca^{2+} release. In a live-cell assay, SPPL3 expression enhanced the BRET between STIM1-YFP and Orai1-myc-Rluc8 (see Fig. S6 in the supplemental material).

Next, we used coimmunoprecipitation to map the domains of STIM1 that influence its association with SPPL3. A series of C-terminal deletions of STIM1 revealed that the cytoplasmic portion of STIM1 inhibits the interaction between STIM1 and SPPL3. The 1–237 STIM1 variant, which contains only the luminal and transmembrane regions of STIM1 (66), displayed a much greater association with SPPL3 than full-length STIM1 (Fig. 8A and B). This inhibitory influence of the cytoplasmic region mapped to at least three regions of STIM1, located between residues 237 and 250, between residues 253 and 535, and between residues 635 and 652. Furthermore, several deletions in the luminal region of STIM1, including the EF hands (residues 63 to 128), the region just N-ter-

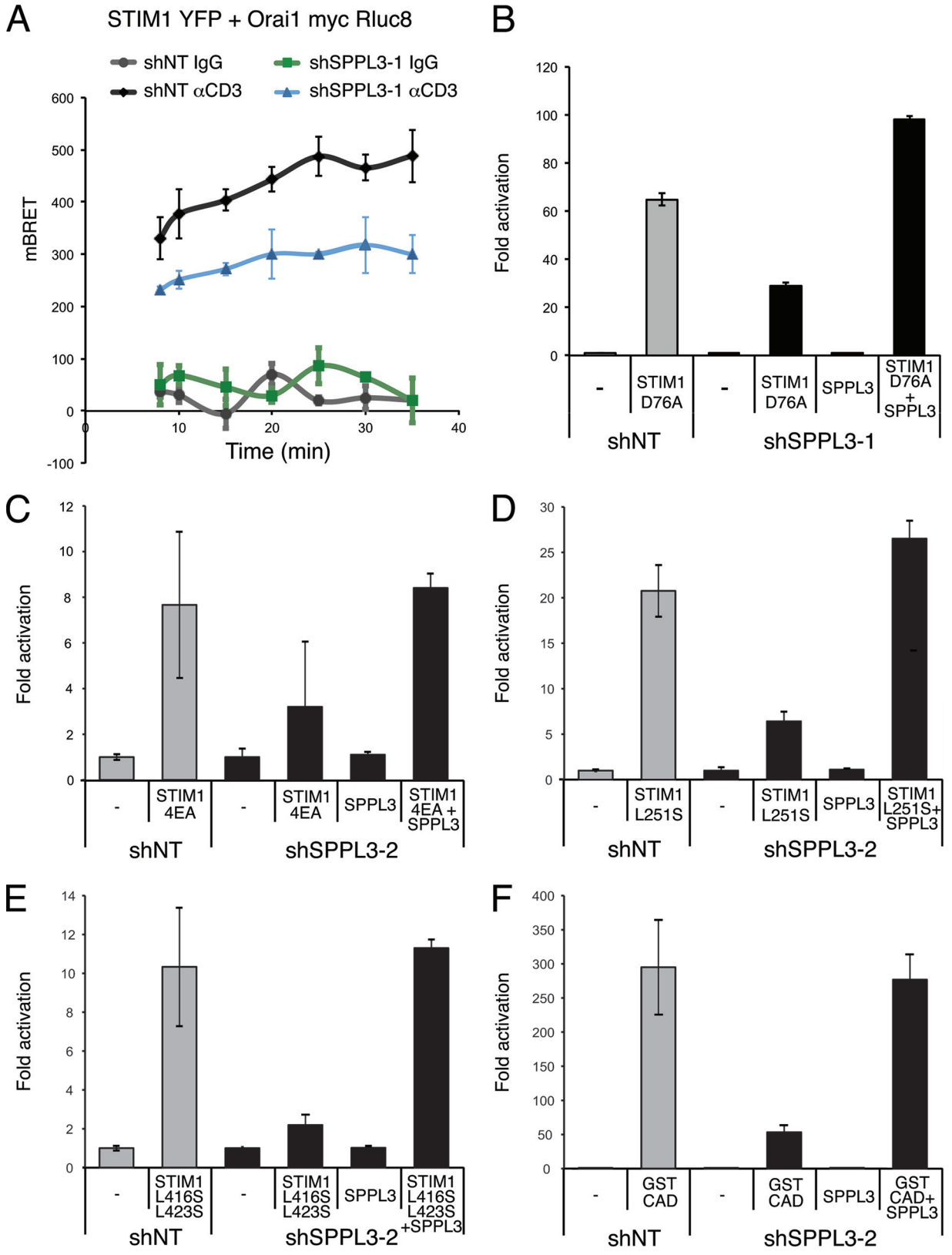

FIG 6 SPPL3 is required for maximal TCR-induced STIM1 association with Orai1, and constitutively active STIM1 variants require SPPL3 for maximal activity. (A) Induced BRET between STIM1-YFP and Orai1-myc-Rluc8 in SPPL3 knockdown (shSPPL3-1) and control (shNT) Jurkat cells after stimulation with 1 μg/ml anti-CD3 and addition of 5 μM coelenterazine-h. As a negative control, cells were treated with IgG. (B to F) NFAT luciferase activities of SPPL3 knockdown Jurkat lines transfected with constitutively active myc-STIM1 D76A (B), myc-STIM1 4EA (C), myc-STIM1 L251S (D), myc-STIM1 L416S L423S (E), or GST-CAD (F). In each panel, SPPL3 knockdown cells were also cotransfected with hairpin-resistant murine SPPL3 to test for rescue of the RNAi effect.

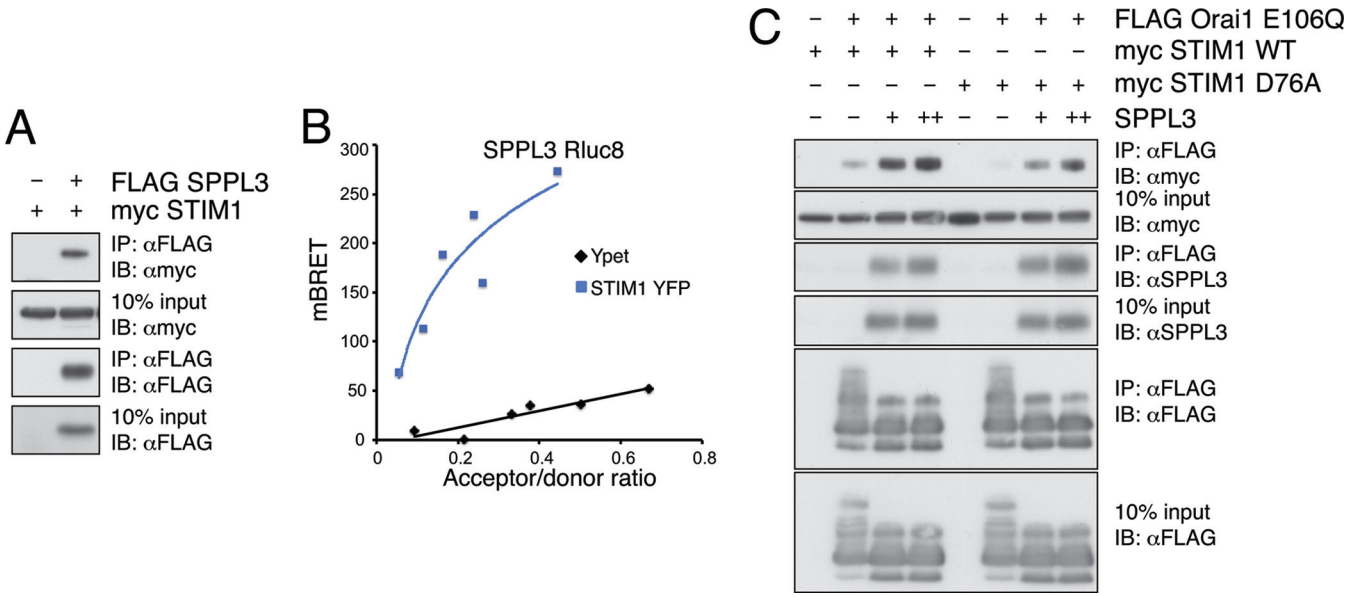

FIG 7 SPPL3 associates with STIM1 and promotes STIM1 binding to Orai1. (A) Coimmunoprecipitation of FLAG-SPPL3 and myc-STIM1 with an anti-FLAG antibody after expression in HEK293T cells. IP, immunoprecipitation; IB, immunoblotting. (B) BRET assay in live HEK293T cells expressing SPPL3-Rluc8 and either STIM1-YFP or Ypet. (C) Co-IP of FLAG-Orai1 E106Q and either myc-STIM1 WT or myc-STIM D76A, in the absence or presence of SPPL3, with an anti-FLAG antibody after expression in HEK293T cells.

minal to the EF hands (residues 29 to 62), and the region between the SAM and transmembrane domains (residues 201 to 213), enhanced the ability of the 1–237 fragment of STIM1 to associate with SPPL3 (Fig. 8C). In contrast, the deletion of the SAM domain (residues 131 to 200) had only a minimal effect on SPPL3 association (Fig. 8C). These results reveal that the interaction between SPPL3 and STIM1 is influenced by multiple, distinct regions of STIM1 that reside in both the ER lumen and the cytosol. In addition, these deletion analyses suggest that the transmembrane domain of STIM1 can minimally mediate association with SPPL3, since this region is present in all variants of the STIM1 1–237 truncation construct that associate with SPPL3.

The fact that CAD-mediated NFAT activation was reduced in SPPL3 knockdown cells (Fig. 6F) suggested that SPPL3 may associate not only with the STIM1 transmembrane domain but also with the CAD, potentially influencing CAD binding to Orai1. Consistent with this prediction, SPPL3 and the GST-CAD fusion associated when coexpressed in HEK293T cells (Fig. 8D). Furthermore, SPPL3 promoted the association of GST-CAD with Orai1 E106Q (Fig. 8E). Taken together, the NFAT reporter activation and association studies suggest that SPPL3 functions in TCR signaling to enhance CAD binding to Orai1 to maximize signal-induced Ca^{2+} influx.

DISCUSSION

Members of the intramembrane aspartyl protease family play a variety of functional roles in the immune system, often dictated by their proteolytic substrate specificities. Our results reveal a function for one of the least understood members of this family, SPPL3, in signaling from the TCR to the NFAT transcription factor. Surprisingly, the activity of SPPL3 in this signaling pathway is independent of its proteolytic activity. SPPL3 functions to enhance Ca^{2+} influx and maximize the sustained increase in the cytoplasmic Ca^{2+} concentration following TCR triggering. SPPL3 knockdown cells display reduced TCR-induced STIM1 and Orai1 association, Ca^{2+} influx, NFAT dephosphorylation, and nuclear translocation, as well as reduced NFAT transcriptional activity.

Our data highlight two steps in TCR signaling that SPPL3 may influence: ER Ca^{2+} store depletion and the association of STIM1 with Orai1 that occurs after the conversion of STIM1 to an active, oligomerized conformation. A potential role for SPPL3 in store depletion is supported by the fact that when overexpressed, SPPL3 clearly induces ER Ca^{2+} release in an IP_3R-independent manner (Fig. 4 and 5). In addition, in unstimulated T cells at physiological expression levels, SPPL3 contributes to the passive ER Ca^{2+} release that is revealed following thapsigargin treatment (Fig. 3F). While one SPPL3 knockdown line consistently displayed defects in TCR-induced ER Ca^{2+} release (Fig. 3), the other line did not, leaving open the possibility that SPPL3 influences ER Ca^{2+} homeostasis or ER store depletion following TCR engagement, possibly as a component of an ER leak channel or by influencing the activity of a channel that contributes to ER Ca^{2+} release. A defect in TCR-induced ER store depletion could explain the reduced STIM1 and Orai1 association, Ca^{2+} influx, NFAT dephosphorylation, and nuclear translocation, and the reduced NFAT transcriptional activity, that we observe in SPPL3 knockdown cells following TCR triggering, since these events occur as a result of the conformational changes in STIM1 that are induced by the signal-dependent release of Ca^{2+} from the ER (26, 64, 65). Indeed, in our BRET assay, which measures the induced association between STIM1 and Orai1 in live T cells, SPPL3 knockdown cells displayed a lower level of STIM1 and Orai1 binding following anti-CD3 treatment than control cells for the duration of the assay (Fig. 6A). Furthermore, SPPL3 knockdown T cells consistently displayed a reduced TCR-induced Ca^{2+} influx rate, peak, and plateau (Fig. 3). Although the effects of SPPL3 knockdown were not as large as those seen with STIM1 and Orai1 knockdown, the failure to sustain maximal cytoplasmic Ca^{2+} levels in SPPL3 knockdown cells

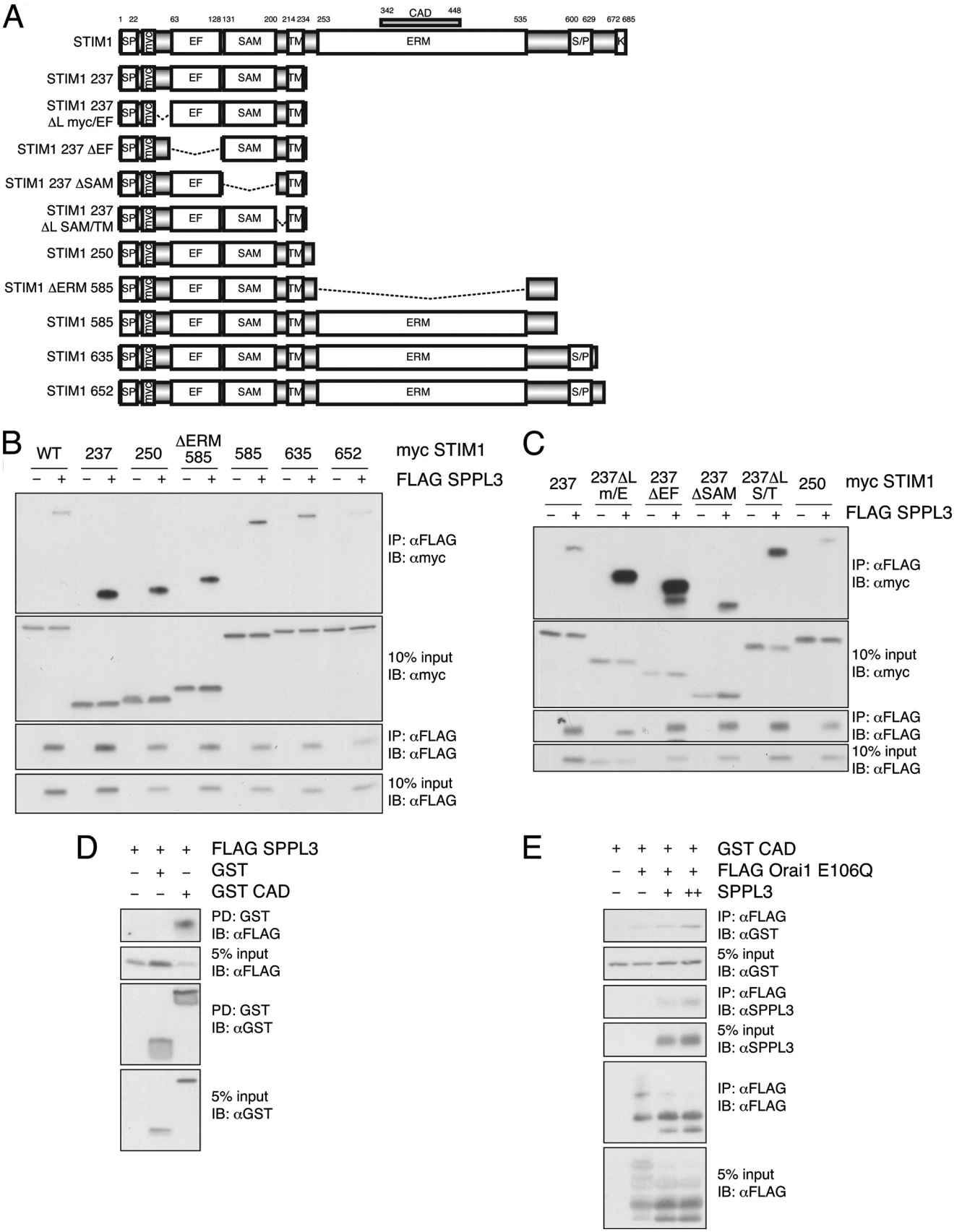

FIG 8 Multiple regions of STIM1 regulate the association with SPPL3, and SPPL3 promotes the binding of the CAD to Orai1. (A) Schematic of myc-STIM1 constructs used in co-IP studies. (B and C) Co-IP of FLAG-SPPL3 and the indicated myc-STIM1 variants, diagramed in panel A, with an anti-FLAG antibody after expression in HEK293T cells. (D) GST pulldown of FLAG-SPPL3 and GST-CAD after expression in HEK293T cells. (E) Co-IP of FLAG-Orai1 E106Q and GST-CAD, in the absence or presence of SPPL3, with an anti-FLAG antibody after expression in HEK293T cells.

likely explains the effect on NFAT induction, since NFAT requires sustained cytoplasmic calcium levels for its activation (67).

An independent role for SPPL3 in maximizing the interaction of STIM1 and Orai1 at a step following the conversion of STIM1 to an active oligomer is supported by the fact that several constitutively active STIM1 mutants, which operate independently of ER Ca^{2+} levels, still required SPPL3 for maximal activity (Fig. 6). Even the activity of the soluble STIM1 CAD construct, which is not tethered to the ER but can still bind and activate Orai1 independently of changes in ER Ca^{2+}, was affected by SPPL3 knockdown. In addition, our immunoprecipitation studies revealed that SPPL3 associates with STIM1 and promotes its interaction with Orai1 (Fig. 7 and 8). Importantly, SPPL3 also promoted the binding of the STIM1 D76A mutant and the CAD to Orai1, findings consistent with a role that is independent of ER Ca^{2+} release. Our deletion and immunoprecipitation analyses indicated that SPPL3 can associate with at least two distinct STIM1 domains, the transmembrane region and the CAD, and interestingly, the association of SPPL3 and STIM1 was influenced by distinct STIM1 regions that reside in the ER lumen and the cytoplasm. Since the CAD becomes exposed as a result of ER store depletion, it is likely that SPPL3 and STIM1 can associate after signaling begins. We have so far been unable to coimmunoprecipitate endogenous STIM1 and SPPL3, so it remains unclear whether SPPL3 and STIM1 associate prior to antigen receptor engagement, after signaling ensues, or both before and during TCR signaling. All of our association studies were performed in the presence of other cellular proteins, so it is possible that SPPL3 associates with the STIM1 CAD or transmembrane region indirectly through other proteins.

Our data do not precisely define how SPPL3 promotes the binding of the STIM1 CAD to Orai1. A wealth of biochemical studies makes it clear that SPPL3 is not absolutely required for the binding of the STIM1 CAD to Orai1 (64, 68), so SPPL3 should be viewed not as an essential component of the SOCE pathway but as a positive modulator. One possibility is that SPPL3 associates transiently with STIM1 during signaling and allosterically promotes a conformation of STIM1 and the CAD that maximizes binding to Orai1. Another possibility is that SPPL3 forms a ternary complex with STIM1 and Orai1 in a signal-dependent manner. TCR signaling does not result in a significant increase in SPPL3 mRNA or protein levels (see Fig. S4A and B in the supplemental material), so it is unlikely that signaling drives the SPPL3–STIM1 interaction through simple mass action. A prediction of the ternary complex model is that SPPL3 should localize to the puncta that mark the ER-plasma membrane junctions where STIM1 and Orai1 interact during SOCE. We have conducted imaging experiments to address this possibility but observe that in thapsigargin-treated cells, SPPL3 remains localized to the ER and does not appear to colocalize with STIM1 in puncta (data not shown). It remains possible that SPPL3 does occupy some or all of the puncta, but at a level below detection by these imaging methods. Further experiments are required to define the mechanism of SPPL3 action in STIM1 and Orai1 binding.

SPPL3 has previously been implicated in central nervous system development by knockdown and overexpression studies in zebrafish (57), and the proteolytic function of SPPL3 appears to be important in this biological context. However, no validated cellular substrates for SPPL3 proteolytic activity have been reported in zebrafish or in any other context, although it has been shown that SPPL3 can cleave the foamy virus envelope protein in a sheddase-like manner (61) and that SPPL3 demonstrates intramembrane protease activity against peptides derived from human cytomegalovirus gpUL40 (69) and bovine prolactin (70), two known substrates of SPP.

Our results clearly reveal a protease-independent function of SPPL3. Notably, studies of the related presenilins have revealed γ-secretase-independent roles in cytoskeletal function (71), membrane trafficking (72), autophagy and protein degradation (73–75), signaling through phosphoinositol 3-kinase (PI3K)/Akt (76) or extracellular signal-regulated kinase (ERK) (77), somite differentiation (78), and even *Dictyostelium* development (79). Presenilins also demonstrate protease-independent effects on Ca^{2+} signaling. Mutations in PS1 and PS2 account for most familial AD cases (29), and PS1 and -2 play an important proteolytic role in AD pathogenesis as catalytic components of γ-secretase through the production of β-amyloid peptides. However, evidence also argues that presenilins contribute to AD by dysregulating Ca^{2+} signaling in a γ-secretase-independent manner by functioning as ER Ca^{2+} leak channels or by affecting the activity of the IP_3R or SERCA (63, 80, 81). Our findings highlight a functional link between presenilins and SPPL3 as intramembrane aspartyl proteases endowed with independent abilities to modulate intracellular Ca^{2+} levels.

The dramatic dose-dependent effect of SPPL3 on NFAT activation by TCR cross-linking raises the possibility that endogenous SPPL3 activity is regulated in the immune system to tune the input-output relationship between receptor triggering and NFAT activity. Future study in the physiological context of an intact immune system will be required to test this possibility and further reveal the biological role of this emerging member of the intramembrane aspartyl protease family.

ACKNOWLEDGMENTS

We thank M. Caterina, S. Desiderio, P. Espenshade, J. Liu, P. Worley, A. Levchenko, M. Vig, C. Haas, T. Kurosaki, J. K. Foskett, R. Rao, M. Katan and M. Presby for reagents, M. Meffert, R. Siliciano, G. Hart, and J. Zhang for the use of equipment, and T. Link, C. Cooper, S. Mehta, S. Desiderio, and M. Meffert for advice and discussions.

This work was supported by National Institutes of Health grant PO1AI072677 and by funds from The Johns Hopkins University Institute for Cell Engineering. S.L.M. was supported by a Dr. Richard and Mavis Fowler and The Foundation for Advanced Research in the Medical Sciences, Inc. (FARMS) Fellowship. J.L.P. is a Leukemia and Lymphoma Society Scholar.

REFERENCES

1. **Crabtree GR, Olson EN.** 2002. NFAT signaling: choreographing the social lives of cells. Cell **109**(Suppl):S67–S79. http://dx.doi.org/10.1016/S0092-8674(02)00699-2.
2. **Hogan PG, Chen L, Nardone J, Rao A.** 2003. Transcriptional regulation by calcium, calcineurin, and NFAT. Genes Dev **17:**2205–2232. http://dx.doi.org/10.1101/gad.1102703.
3. **Macian F.** 2005. NFAT proteins: key regulators of T-cell development and function. Nat Rev Immunol **5:**472–484. http://dx.doi.org/10.1038/nri1632.
4. **Lewis RS.** 2011. Store-operated calcium channels: new perspectives on mechanism and function. Cold Spring Harb Perspect Biol **3**(12):a003970. http://dx.doi.org/10.1101/cshperspect.a003970.
5. **Stathopulos PB, Li GY, Plevin MJ, Ames JB, Ikura M.** 2006. Stored Ca^{2+} depletion-induced oligomerization of stromal interaction molecule 1 (STIM1) via the EF-SAM region: an initiation mechanism for capacitive Ca^{2+} entry. J Biol Chem **281:**35855–35862. http://dx.doi.org/10.1074/jbc.M608247200.
6. **Stathopulos PB, Zheng L, Li GY, Plevin MJ, Ikura M.** 2008. Structural and mechanistic insights into STIM1-mediated initiation of store-

operated calcium entry. Cell **135:**110–122. http://dx.doi.org/10.1016/j.cell.2008.08.006.
7. **Zheng L, Stathopulos PB, Li GY, Ikura M.** 2008. Biophysical characterization of the EF-hand and SAM domain containing Ca^{2+} sensory region of STIM1 and STIM2. Biochem Biophys Res Commun **369:**240–246. http://dx.doi.org/10.1016/j.bbrc.2007.12.129.
8. **Stathopulos PB, Zheng L, Ikura M.** 2009. Stromal interaction molecule (STIM) 1 and STIM2 calcium sensing regions exhibit distinct unfolding and oligomerization kinetics. J Biol Chem **284:**728–732. http://dx.doi.org/10.1074/jbc.C800178200.
9. **Zheng L, Stathopulos PB, Schindl R, Li GY, Romanin C, Ikura M.** 2011. Auto-inhibitory role of the EF-SAM domain of STIM proteins in store-operated calcium entry. Proc Natl Acad Sci U S A **108:**1337–1342. http://dx.doi.org/10.1073/pnas.1015125108.
10. **Muik M, Fahrner M, Schindl R, Stathopulos P, Frischauf I, Derler I, Plenk P, Lackner B, Groschner K, Ikura M, Romanin C.** 2011. STIM1 couples to ORAI1 via an intramolecular transition into an extended conformation. EMBO J **30:**1678–1689. http://dx.doi.org/10.1038/emboj.2011.79.
11. **Yang X, Jin H, Cai X, Li S, Shen Y.** 2012. Structural and mechanistic insights into the activation of stromal interaction molecule 1 (STIM1). Proc Natl Acad Sci U S A **109:**5657–5662. http://dx.doi.org/10.1073/pnas.1118947109.
12. **Park CY, Hoover PJ, Mullins FM, Bachhawat P, Covington ED, Raunser S, Walz T, Garcia KC, Dolmetsch RE, Lewis RS.** 2009. STIM1 clusters and activates CRAC channels via direct binding of a cytosolic domain to Orai1. Cell **136:**876–890. http://dx.doi.org/10.1016/j.cell.2009.02.014.
13. **Yuan JP, Zeng W, Dorwart MR, Choi YJ, Worley PF, Muallem S.** 2009. SOAR and the polybasic STIM1 domains gate and regulate Orai channels. Nat Cell Biol **11:**337–343. http://dx.doi.org/10.1038/ncb1842.
14. **Kawasaki T, Lange I, Feske S.** 2009. A minimal regulatory domain in the C terminus of STIM1 binds to and activates ORAI1 CRAC channels. Biochem Biophys Res Commun **385:**49–54. http://dx.doi.org/10.1016/j.bbrc.2009.05.020.
15. **Korzeniowski MK, Manjarres IM, Varnai P, Balla T.** 2010. Activation of STIM1-Orai1 involves an intramolecular switching mechanism. Sci Signal **3:**ra82. http://dx.doi.org/10.1126/scisignal.2001122.
16. **Muik M, Fahrner M, Derler I, Schindl R, Bergsmann J, Frischauf I, Groschner K, Romanin C.** 2009. A cytosolic homomerization and a modulatory domain within STIM1 C terminus determine coupling to ORAI1 channels. J Biol Chem **284:**8421–8426. http://dx.doi.org/10.1074/jbc.C800229200.
17. **Zhou Y, Srinivasan P, Razavi S, Seymour S, Meraner P, Gudlur A, Stathopulos PB, Ikura M, Rao A, Hogan PG.** 2013. Initial activation of STIM1, the regulator of store-operated calcium entry. Nat Struct Mol Biol **20:**973–981. http://dx.doi.org/10.1038/nsmb.2625.
18. **Liou J, Kim ML, Heo WD, Jones JT, Myers JW, Ferrell JE, Jr, Meyer T.** 2005. STIM is a Ca^{2+} sensor essential for Ca^{2+}-store-depletion-triggered Ca^{2+} influx. Curr Biol **15:**1235–1241. http://dx.doi.org/10.1016/j.cub.2005.05.055.
19. **Roos J, DiGregorio PJ, Yeromin AV, Ohlsen K, Lioudyno M, Zhang S, Safrina O, Kozak JA, Wagner SL, Cahalan MD, Velicelebi G, Stauderman KA.** 2005. STIM1, an essential and conserved component of store-operated Ca^{2+} channel function. J Cell Biol **169:**435–445. http://dx.doi.org/10.1083/jcb.200502019.
20. **Vig M, Peinelt C, Beck A, Koomoa DL, Rabah D, Koblan-Huberson M, Kraft S, Turner H, Fleig A, Penner R, Kinet JP.** 2006. CRACM1 is a plasma membrane protein essential for store-operated Ca^{2+} entry. Science **312:**1220–1223. http://dx.doi.org/10.1126/science.1127883.
21. **Zhang SL, Yeromin AV, Zhang XH, Yu Y, Safrina O, Penna A, Roos J, Stauderman KA, Cahalan MD.** 2006. Genome-wide RNAi screen of Ca^{2+} influx identifies genes that regulate Ca^{2+} release-activated Ca^{2+} channel activity. Proc Natl Acad Sci U S A **103:**9357–9362. http://dx.doi.org/10.1073/pnas.0603161103.
22. **Feske S, Gwack Y, Prakriya M, Srikanth S, Puppel SH, Tanasa B, Hogan PG, Lewis RS, Daly M, Rao A.** 2006. A mutation in Orai1 causes immune deficiency by abrogating CRAC channel function. Nature **441:**179–185. http://dx.doi.org/10.1038/nature04702.
23. **Yeromin AV, Zhang SL, Jiang W, Yu Y, Safrina O, Cahalan MD.** 2006. Molecular identification of the CRAC channel by altered ion selectivity in a mutant of Orai. Nature **443:**226–229. http://dx.doi.org/10.1038/nature05108.
24. **Vig M, Beck A, Billingsley JM, Lis A, Parvez S, Peinelt C, Koomoa DL, Soboloff J, Gill DL, Fleig A, Kinet JP, Penner R.** 2006. CRACM1 multimers form the ion-selective pore of the CRAC channel. Curr Biol **16:**2073–2079. http://dx.doi.org/10.1016/j.cub.2006.08.085.
25. **Prakriya M, Feske S, Gwack Y, Srikanth S, Rao A, Hogan PG.** 2006. Orai1 is an essential pore subunit of the CRAC channel. Nature **443:**230–233. http://dx.doi.org/10.1038/nature05122.
26. **Hogan PG, Lewis RS, Rao A.** 2010. Molecular basis of calcium signaling in lymphocytes: STIM and ORAI. Annu Rev Immunol **28:**491–533. http://dx.doi.org/10.1146/annurev.immunol.021908.132550.
27. **Srikanth S, Gwack Y.** 2012. Orai1, STIM1, and their associating partners. J Physiol **590**(Part 17):4169–4177. http://dx.doi.org/10.1113/jphysiol.2012.231522.
28. **Voss M, Schroder B, Fluhrer R.** 2013. Mechanism, specificity, and physiology of signal peptide peptidase (SPP) and SPP-like proteases. Biochim Biophys Acta **1828:**2828–2839. http://dx.doi.org/10.1016/j.bbamem.2013.03.033.
29. **Ho A, Shen J.** 2011. Presenilins in synaptic function and disease. Trends Mol Med **17:**617–624. http://dx.doi.org/10.1016/j.molmed.2011.06.002.
30. **Weihofen A, Binns K, Lemberg MK, Ashman K, Martoglio B.** 2002. Identification of signal peptide peptidase, a presenilin-type aspartic protease. Science **296:**2215–2218. http://dx.doi.org/10.1126/science.1070925.
31. **El Hage F, Stroobant V, Vergnon I, Baurain JF, Echchakir H, Lazar V, Chouaib S, Coulie PG, Mami-Chouaib F.** 2008. Preprocalcitonin signal peptide generates a cytotoxic T lymphocyte-defined tumor epitope processed by a proteasome-independent pathway. Proc Natl Acad Sci U S A **105:**10119–10124. http://dx.doi.org/10.1073/pnas.0802753105.
32. **Schneppenheim J, Dressel R, Huttl S, Lullmann-Rauch R, Engelke M, Dittmann K, Wienands J, Eskelinen EL, Hermans-Borgmeyer I, Fluhrer R, Saftig P, Schroder B.** 2013. The intramembrane protease SPPL2a promotes B cell development and controls endosomal traffic by cleavage of the invariant chain. J Exp Med **210:**41–58. http://dx.doi.org/10.1084/jem.20121069.
33. **Bergmann H, Yabas M, Short A, Miosge L, Barthel N, Teh CE, Roots CM, Bull KR, Jeelall Y, Horikawa K, Whittle B, Balakishnan B, Sjollema G, Bertram EM, Mackay F, Rimmer AJ, Cornall RJ, Field MA, Andrews TD, Goodnow CC, Enders A.** 2013. B cell survival, surface BCR and BAFFR expression, CD74 metabolism, and $CD8^-$ dendritic cells require the intramembrane endopeptidase SPPL2A. J Exp Med **210:**31–40. http://dx.doi.org/10.1084/jem.20121076.
34. **Beisner DR, Langerak P, Parker AE, Dahlberg C, Otero FJ, Sutton SE, Poirot L, Barnes W, Young MA, Niessen S, Wiltshire T, Bodendorf U, Martoglio B, Cravatt B, Cooke MP.** 2013. The intramembrane protease Sppl2a is required for B cell and DC development and survival via cleavage of the invariant chain. J Exp Med **210:**23–30. http://dx.doi.org/10.1084/jem.20121072.
35. **Lückerath K, Kirkin V, Melzer IM, Thalheimer FB, Siele D, Milani W, Adler T, Aguilar-Pimentel A, Horsch M, Michel G, Beckers J, Busch DH, Ollert M, Gailus-Durner V, Fuchs H, Hrabe de Angelis M, Staal FJ, Rajalingam K, Hueber AO, Strobl LJ, Zimber-Strobl U, Zornig M.** 2011. Immune modulation by Fas ligand reverse signaling: lymphocyte proliferation is attenuated by the intracellular Fas ligand domain. Blood **117:**519–529. http://dx.doi.org/10.1182/blood-2010-07-292722.
36. **Friedmann E, Hauben E, Maylandt K, Schleeger S, Vreugde S, Lichtenthaler SF, Kuhn PH, Stauffer D, Rovelli G, Martoglio B.** 2006. SPPL2a and SPPL2b promote intramembrane proteolysis of TNFα in activated dendritic cells to trigger IL-12 production. Nat Cell Biol **8:**843–848. http://dx.doi.org/10.1038/ncb1440.
37. **Lamason RL, Lew SM, Pomerantz JL.** 2010. Transcriptional target-based expression cloning of immunoregulatory molecules. Immunol Res **47:**172–178. http://dx.doi.org/10.1007/s12026-009-8148-z.
38. **Pomerantz JL, Denny EM, Baltimore D.** 2002. CARD11 mediates factor-specific activation of NF-κB by the T cell receptor complex. EMBO J **21:**5184–5194. http://dx.doi.org/10.1093/emboj/cdf505.
39. **Shibasaki F, Price ER, Milan D, McKeon F.** 1996. Role of kinases and the phosphatase calcineurin in the nuclear shuttling of transcription factor NF-AT4. Nature **382:**370–373. http://dx.doi.org/10.1038/382370a0.
40. **Huang GN, Zeng W, Kim JY, Yuan JP, Han L, Muallem S, Worley PF.** 2006. STIM1 carboxyl-terminus activates native SOC, I_{crac} and TRPC1 channels. Nat Cell Biol **8:**1003–1010. http://dx.doi.org/10.1038/ncb1454.
41. **Everett KL, Bunney TD, Yoon Y, Rodrigues-Lima F, Harris R, Driscoll PC, Abe K, Fuchs H, de Angelis MH, Yu P, Cho W, Katan M.** 2009. Characterization of phospholipase Cγ enzymes with gain-of-function

mutations. J Biol Chem **284:**23083–23093. http://dx.doi.org/10.1074/jbc.M109.019265.
42. **Youn HD, Chatila TA, Liu JO.** 2000. Integration of calcineurin and MEF2 signals by the coactivator p300 during T-cell apoptosis. EMBO J **19:**4323–4331. http://dx.doi.org/10.1093/emboj/19.16.4323.
43. **Monticelli S, Rao A.** 2002. NFAT1 and NFAT2 are positive regulators of IL-4 gene transcription. Eur J Immunol **32:**2971–2978. http://dx.doi.org/10.1002/1521-4141(2002010)32:10<2971::AID-IMMU2971>3.0.CO;2-G.
44. **Palmer AE, Jin C, Reed JC, Tsien RY.** 2004. Bcl-2-mediated alterations in endoplasmic reticulum Ca^{2+} analyzed with an improved genetically encoded fluorescent sensor. Proc Natl Acad Sci U S A **101:**17404–17409. http://dx.doi.org/10.1073/pnas.0408030101.
45. **McCully RR, Pomerantz JL.** 2008. The protein kinase C-responsive inhibitory domain of CARD11 functions in NF-κB activation to regulate the association of multiple signaling cofactors that differentially depend on Bcl10 and MALT1 for association. Mol Cell Biol **28:**5668–5686. http://dx.doi.org/10.1128/MCB.00418-08.
46. **Sugawara H, Kurosaki M, Takata M, Kurosaki T.** 1997. Genetic evidence for involvement of type 1, type 2 and type 3 inositol 1,4,5-trisphosphate receptors in signal transduction through the B-cell antigen receptor. EMBO J **16:**3078–3088. http://dx.doi.org/10.1093/emboj/16.11.3078.
47. **Chan W, Schaffer TB, Pomerantz JL.** 2013. A quantitative signaling screen identifies CARD11 mutations in the CARD and LATCH domains that induce Bcl10 ubiquitination and human lymphoma cell survival. Mol Cell Biol **33:**429–443. http://dx.doi.org/10.1128/MCB.00850-12.
48. **Zelenski NG, Rawson RB, Brown MS, Goldstein JL.** 1999. Membrane topology of S2P, a protein required for intramembranous cleavage of sterol regulatory element-binding proteins. J Biol Chem **274:**21973–21980. http://dx.doi.org/10.1074/jbc.274.31.21973.
49. **Franklin R, Sale JE.** 2006. Transient transfection of DT40. Subcell Biochem **40:**379–382.
50. **Lamason RL, Kupfer A, Pomerantz JL.** 2010. The dynamic distribution of CARD11 at the immunological synapse is regulated by the inhibitor kinesin GAKIN. Mol Cell **40:**798–809. http://dx.doi.org/10.1016/j.molcel.2010.11.007.
51. **Caraveo G, van Rossum DB, Patterson RL, Snyder SH, Desiderio S.** 2006. Action of TFII-I outside the nucleus as an inhibitor of agonist-induced calcium entry. Science **314:**122–125. http://dx.doi.org/10.1126/science.1127815.
52. **Feng M, Grice DM, Faddy HM, Nguyen N, Leitch S, Wang Y, Muend S, Kenny PA, Sukumar S, Roberts-Thomson SJ, Monteith GR, Rao R.** 2010. Store-independent activation of Orai1 by SPCA2 in mammary tumors. Cell **143:**84–98. http://dx.doi.org/10.1016/j.cell.2010.08.040.
53. **Palmer AE, Tsien RY.** 2006. Measuring calcium signaling using genetically targetable fluorescent indicators. Nat Protoc **1:**1057–1065. http://dx.doi.org/10.1038/nprot.2006.172.
54. **McCombs JE, Gibson EA, Palmer AE.** 2010. Using a genetically targeted sensor to investigate the role of presenilin-1 in ER Ca^{2+} levels and dynamics. Mol Biosyst **6:**1640–1649. http://dx.doi.org/10.1039/c001975e.
55. **Mehta S, Zhang J.** 2014. Using a genetically encoded FRET-based reporter to visualize calcineurin phosphatase activity in living cells. Methods Mol Biol **1071:**139–149. http://dx.doi.org/10.1007/978-1-62703-622-1_11.
56. **Hamdan FF, Percherancier Y, Breton B, Bouvier M.** 2006. Monitoring protein-protein interactions in living cells by bioluminescence resonance energy transfer (BRET). Curr Protoc Neurosci Chapter 5:Unit 5.23. http://dx.doi.org/10.1002/0471142301.ns0523s34.
57. **Krawitz P, Haffner C, Fluhrer R, Steiner H, Schmid B, Haass C.** 2005. Differential localization and identification of a critical aspartate suggest non-redundant proteolytic functions of the presenilin homologues SPPL2b and SPPL3. J Biol Chem **280:**39515–39523. http://dx.doi.org/10.1074/jbc.M501645200.
58. **Ponting CP, Hutton M, Nyborg A, Baker M, Jansen K, Golde TE.** 2002. Identification of a novel family of presenilin homologues. Hum Mol Genet **11:**1037–1044. http://dx.doi.org/10.1093/hmg/11.9.1037.
59. **Grigorenko AP, Moliaka YK, Korovaitseva GI, Rogaev EI.** 2002. Novel class of polytopic proteins with domains associated with putative protease activity. Biochemistry (Mosc) **67:**826–835. http://dx.doi.org/10.1023/A:1016365227942.
60. **Fluhrer R, Steiner H, Haass C.** 2009. Intramembrane proteolysis by signal peptide peptidases: a comparative discussion of GXGD-type aspartyl proteases. J Biol Chem **284:**13975–13979. http://dx.doi.org/10.1074/jbc.R800040200.
61. **Voss M, Fukumori A, Kuhn PH, Kunzel U, Klier B, Grammer G, Haug-Kroper M, Kremmer E, Lichtenthaler SF, Steiner H, Schroder B, Haass C, Fluhrer R.** 2012. Foamy virus envelope protein is a substrate for signal peptide peptidase-like 3 (SPPL3). J Biol Chem **287:**43401–43409. http://dx.doi.org/10.1074/jbc.M112.371369.
62. **Rao A, Luo C, Hogan PG.** 1997. Transcription factors of the NFAT family: regulation and function. Annu Rev Immunol **15:**707–747. http://dx.doi.org/10.1146/annurev.immunol.15.1.707.
63. **Cheung KH, Mei L, Mak DO, Hayashi I, Iwatsubo T, Kang DE, Foskett JK.** 2010. Gain-of-function enhancement of IP3 receptor modal gating by familial Alzheimer's disease-linked presenilin mutants in human cells and mouse neurons. Sci Signal **3:**ra22. http://dx.doi.org/10.1126/scisignal.2000818.
64. **Soboloff J, Rothberg BS, Madesh M, Gill DL.** 2012. STIM proteins: dynamic calcium signal transducers. Nat Rev Mol Cell Biol **13:**549–565. http://dx.doi.org/10.1038/nrm3414.
65. **Shaw PJ, Qu B, Hoth M, Feske S.** 2013. Molecular regulation of CRAC channels and their role in lymphocyte function. Cell Mol Life Sci **70:**2637–2656. http://dx.doi.org/10.1007/s00018-012-1175-2.
66. **Covington ED, Wu MM, Lewis RS.** 2010. Essential role for the CRAC activation domain in store-dependent oligomerization of STIM1. Mol Biol Cell **21:**1897–1907. http://dx.doi.org/10.1091/mbc.E10-02-0145.
67. **Dolmetsch RE, Lewis RS, Goodnow CC, Healy JI.** 1997. Differential activation of transcription factors induced by Ca^{2+} response amplitude and duration. Nature **386:**855–858. http://dx.doi.org/10.1038/386855a0.
68. **Zhou Y, Meraner P, Kwon HT, Machnes D, Oh-hora M, Zimmer J, Huang Y, Stura A, Rao A, Hogan PG.** 2010. STIM1 gates the store-operated calcium channel ORAI1 in vitro. Nat Struct Mol Biol **17:**112–116. http://dx.doi.org/10.1038/nsmb.1724.
69. **Nyborg AC, Ladd TB, Jansen K, Kukar T, Golde TE.** 2006. Intramembrane proteolytic cleavage by human signal peptide peptidase like 3 and malaria signal peptide peptidase. FASEB J **20:**1671–1679. http://dx.doi.org/10.1096/fj.06-5762com.
70. **Narayanan S, Sato T, Wolfe MS.** 2007. A C-terminal region of signal peptide peptidase defines a functional domain for intramembrane aspartic protease catalysis. J Biol Chem **282:**20172–20179. http://dx.doi.org/10.1074/jbc.M701536200.
71. **Khandelwal A, Chandu D, Roe CM, Kopan R, Quatrano RS.** 2007. Moonlighting activity of presenilin in plants is independent of gamma-secretase and evolutionarily conserved. Proc Natl Acad Sci U S A **104:**13337–13342. http://dx.doi.org/10.1073/pnas.0702038104.
72. **Wrigley JD, Schurov I, Nunn EJ, Martin AC, Clarke EE, Ellis S, Bonnert TP, Shearman MS, Beher D.** 2005. Functional overexpression of gamma-secretase reveals protease-independent trafficking functions and a critical role of lipids for protease activity. J Biol Chem **280:**12523–12535. http://dx.doi.org/10.1074/jbc.M413086200.
73. **Kang DE, Soriano S, Xia X, Eberhart CG, De Strooper B, Zheng H, Koo EH.** 2002. Presenilin couples the paired phosphorylation of beta-catenin independent of axin: implications for beta-catenin activation in tumorigenesis. Cell **110:**751–762. http://dx.doi.org/10.1016/S0092-8674(02)00970-4.
74. **Esselens C, Oorschot V, Baert V, Raemaekers T, Spittaels K, Serneels L, Zheng H, Saftig P, De Strooper B, Klumperman J, Annaert W.** 2004. Presenilin 1 mediates the turnover of telencephalin in hippocampal neurons via an autophagic degradative pathway. J Cell Biol **166:**1041–1054. http://dx.doi.org/10.1083/jcb.200406060.
75. **Wilson CA, Murphy DD, Giasson BI, Zhang B, Trojanowski JQ, Lee VM.** 2004. Degradative organelles containing mislocalized alpha-and beta-synuclein proliferate in presenilin-1 null neurons. J Cell Biol **165:**335–346. http://dx.doi.org/10.1083/jcb.200403061.
76. **Baki L, Shioi J, Wen P, Shao Z, Schwarzman A, Gama-Sosa M, Neve R, Robakis NK.** 2004. PS1 activates PI3K thus inhibiting GSK-3 activity and tau overphosphorylation: effects of FAD mutations. EMBO J **23:**2586–2596. http://dx.doi.org/10.1038/sj.emboj.7600251.
77. **Kang DE, Yoon IS, Repetto E, Busse T, Yermian N, Ie L, Koo EH.** 2005. Presenilins mediate phosphatidylinositol 3-kinase/AKT and ERK activation via select signaling receptors. Selectivity of PS2 in platelet-derived growth factor signaling. J Biol Chem **280:**31537–31547. http://dx.doi.org/10.1074/jbc.M500833200.
78. **Huppert SS, Ilagan MX, De Strooper B, Kopan R.** 2005. Analysis of Notch function in presomitic mesoderm suggests a gamma-secretase-independent role for presenilins in somite differentiation. Dev Cell **8:**677–688. http://dx.doi.org/10.1016/j.devcel.2005.02.019.

79. **Ludtmann MH, Otto GP, Schilde C, Chen ZH, Allan CY, Brace S, Beesley PW, Kimmel AR, Fisher P, Killick R, Williams RS.** 2014. An ancestral non-proteolytic role for presenilin proteins in multicellular development of the social amoeba *Dictyostelium discoideum*. J Cell Sci **127:** 1576–1584. http://dx.doi.org/10.1242/jcs.140939.
80. **Green KN, Demuro A, Akbari Y, Hitt BD, Smith IF, Parker I, LaFerla FM.** 2008. SERCA pump activity is physiologically regulated by presenilin and regulates amyloid beta production. J Cell Biol **181:**1107–1116. http://dx.doi.org/10.1083/jcb.200706171.
81. **Tu H, Nelson O, Bezprozvanny A, Wang Z, Lee SF, Hao YH, Serneels L, De Strooper B, Yu G, Bezprozvanny I.** 2006. Presenilins form ER Ca^{2+} leak channels, a function disrupted by familial Alzheimer's disease-linked mutations. Cell **126:**981–993. http://dx.doi.org/10.1016/j.cell.2006.06.059.